Time Domain Double Diffraction at a Pair of Coplanar Skew Edges

Filippo Capolino, *Senior Member, IEEE,* and Matteo Albani, *Member, IEEE*

***Abstract*—This study aims at describing the field propagation in terms of pulsed rays, that are particularly advantageous when dealing with short-pulse excitations. In the framework of the Geometrical Theory of Diffraction we augment Geometrical Optics and uniform singly diffracted field solutions available in the time domain (TD), by TD doubly diffracted (DD) rays, that are expressed in simple closed forms. Impulsive double diffraction at a pair of coplanar edges is here formulated directly in the TD, as a double superposition of impulsive spherical waves. *Nonuniform* and *uniform* wavefront approximations for TD-DD fields are determined in closed form, defining two novel TD transition functions. The scalar case with either hard or soft boundary conditions is analyzed first, and then used to build an electromagnetic dyadic DD coefficient for a pair of coplanar edges with perfectly conducting faces. Particular attention is given to the definition of TD transition regions, i.e., the elliptical regions where the TD-DD field does not exhibit a ray optical behavior. The compensation mechanism by which the TD-DD fields repair the discontinuity introduced by singly diffracted fields at their shadow boundaries is also analyzed in detail. Our result for the TD-DD field excited by an impulsive spherical wave is valid only for *early times*, at and close to (behind) the DD ray wavefront. The TD-DD field response to a more general pulsed excitation is obtained via convolution, and if the exciting signal has no low-frequency components the range of validity of the resulting pulsed response is enlarged to later observation times behind the wavefront.**

***Index Terms*—Diffraction, electromagnetic transient analysis, ray tracing, time domain (TD) analysis, transient propagation, transient scattering, wedges.**

I. Introduction

WAVE propagation in terms of rays, obtained using high-frequency approximations, is an efficient tool in a variety of applications in the frequency domain (FD). Studies of ray propagation directly in the time domain (TD) have also been carried out in the past, since they offer a compact description of the field propagation when excited by short-pulses. In particular, previous studies of TD Geometrical Optics (GO) and TD diffracted fields have been presented in [1]–[3]. In [4]–[6], a spectral theory of transients was presented to represent TD fields in terms of their spectral components, also systematizing the various approximations that can be obtained from that representation. Successively, TD diffraction by wedges have been studied in [7] in a Geometrical Theory of Diffraction (GTD) framework, and in a systematic way in [8]–[10], by using analytic signals, thus allowing the time to be a complex variable. TD wedge diffraction in a uniform theory of diffraction (UTD) framework using analytic signals has been presented in [11]. In this paper a TD doubly diffracted (DD) field at a pair of coplanar skew edges is presented, with impulsive spherical source and observation at a finite distance. This is developed to augment the GO and singly diffracted (SD) fields in a UTD framework. Therefore, the total field is represented here as

$$\hat{\psi}^{\mathrm{tot}} = \hat{\psi}^{\mathrm{GO}} + \hat{\psi}_1^d + \hat{\psi}_2^d + \hat{\psi}_{12}^{\mathrm{dd}} + \hat{\psi}_{21}^{\mathrm{dd}} \tag{1}$$

where $\hat{\psi}^{\mathrm{GO}}$ is the GO term, $\hat{\psi}_i^d$ are the SD fields arising from edges $i = 1, 2$, that are depicted in Fig. 1, and $\hat{\psi}_{ij}^{\mathrm{dd}}$ is the DD field, i.e., the field diffracted at edge i and subsequently diffracted at edge $j (ij = 12, 21)$, as depicted in Fig. 2. As usual in a GTD description, each field contribution is defined only in its lit region; thus, it is bounded by shadow boundaries (SBs). For example, referring to Fig. 1, the GO field contribution from source A exists only above its $\mathrm{SB}_A^{\mathrm{GO}}$. Also, as long as the source A lies above the SB^d plane containing the two edges, a SD field $\hat{\psi}_2^d$ is excited at edge 2. Therefore, when the source moves from A to B and crosses the SB^d, the field $\hat{\psi}_2^d$ abruptly disappears.

Analogously, the SD field contribution $\hat{\psi}_1^d$ abruptly disappears when the observer P crosses the SB^d. Indeed, ray descriptions limited to GO and SD field contributions present abrupt discontinuities at SBs of SD rays, that occur at SB^d in Fig. 1. Furthermore, the GO + UTDSD field description is not satisfactory in shadow regions where neither GO nor UTD rays are traced, e.g., when both source B and observer P are below the SB^d plane; thus, predicting a vanishing field. The augmentation by DD fields solves these impairments.

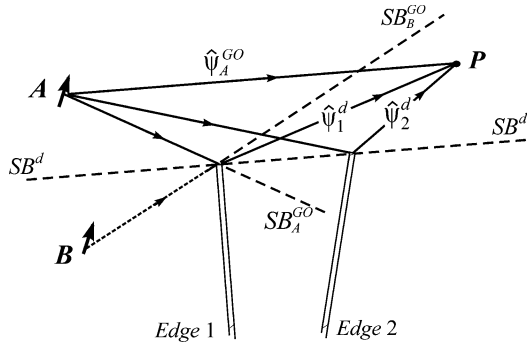

Fig. 1. GTD ray field description including GO $\hat{\psi}^{\mathrm{GO}}$, SD $\hat{\psi}_i^d$, with $i = 1, 2$, field contributions. Two source locations A and B are considered. The region of definition of each ray field contribution is bounded by a shadow boundary (SB) plane, e.g., the GO field from B exists only above its $\mathrm{SB}_B^{\mathrm{GO}}$, and therefore cannot excite the field $\hat{\psi}_2^d$ diffracted at edge 2. Equivalently, the field $\hat{\psi}_2^d$ is excited only when the source point B is above the SB^d plane. The DD field mechanism 12 is shown in Fig. 2.

Manuscript received January 8, 2003; revised January 2, 2004.

F. Capolino is with the Department of Information Engineering, University of Siena, 53100 Siena, Italy (e-mail: capolino@dii.unisi.it).

M. Albani is with the Department of Matter Physics and Advanced Physical Technologies, University of Messina, 98166 Messina, Italy (e-mail: malbani@ingegneria.unime.it).

Digital Object Identifier 10.1109/TAP.2005.844457

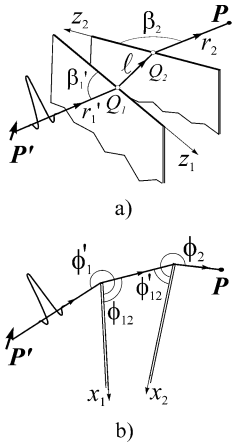

Fig. 2. Geometry of the two half planes and DD ray-fixed coordinate systems. (a) Angles with respect to the edges. (b) Transverse angles.

The TD-DD field formulation is constructed via spectral synthesis, as it was done for the FD-DD field recently developed in [12]–[14] for point source time-harmonic excitation, and in [15] for line source time-harmonic excitation. In Section II, the spectral synthesis is completely rephrased in the TD via a continuous superposition of elementary impulsive spherical sources. Next, in Section III, the resulting double spectral integral is evaluated under the wavefront approximation (here denoted by *nonuniform*), i.e., for space-time location at and immediately behind the DD wavefront. However, this result suffers of the usual impairments of the GTD, i.e., it is unbounded at the SBs of SD fields. Therefore, a *uniform wavefront approximation* for the TD-DD field is then carried out in terms of canonical spectral integrals that are evaluated in closed form defining two novel TD transition functions for TD-DD fields. These TD canonical functions have also a broader application and can be applied to other diffraction problems with pulse excitation (see [16]). Furthermore, the present result is cast in such a way that the *uniform wavefront approximation* reduces to the *nonuniform* one out of DD transition regions. In Section IV, it is shown that the present TD uniform result can be obtained also by inverse Fourier transforming the high-frequency uniform approximation for the FD-DD field in [12] which is conveniently expressed in terms of generalized Fresnel integrals [17]. For describing the electromagnetic DD fields at coplanar skew edges with perfectly conducting faces, in Section V the scalar DD coefficients determined in Section III are used to obtain a dyadic diffraction coefficient. Section VI illustrates how our *uniform approximation* for TD-DD fields compensates for the discontinuities of SD fields at their SBs, thus providing a continuous field. Particular attention is given to the physical interpretation in the TD of the FD transition regions, and to the definition of the TD transition regions. Furthermore, DD fields at a flat plate are obtained in Section VII as a particular case of the solution of Section III. Their nonuniform versions coincide with the second order diffraction mechanisms described in [18], [19] for a strip. In Section VIII, numerical results illustrate the various transitional behaviors that are shown analytically in Section VI.

In principle, the present TD-DD result is valid only for *early times*, on and close to (behind) the DD ray wavefronts for the following reasons. First, it has been obtained by a suitable wavefront approximation, as demonstrated in [4]–[6] in general terms. Second, it is shown that the present uniform wavefront approximation for TD-DD field is the exact Fourier transform of the uniform expression for FD-DD field obtained in [12], whose accuracy has been proved at high-frequency in [12], [15], [13] against Method of Moments (MoM) and measurement results in various geometric configurations. The TD-DD field response to a general pulsed excitation is obtained via convolution between the exciting pulse and the impulsive DD response, as shown in Section VIII. When the exciting signal has no low-frequency components and is dominated by high frequencies, the range of validity of the resulting pulsed response is extended to later observation times behind the wavefront.

II. DD Field Spectral Synthesis

Let us consider a pair of half planes with soft/hard boundary conditions (BC) and coplanar edges, illuminated by a spherical source. It is useful to define spherical (r_i, β_i, ϕ_i) ray fixed coordinate systems at each edge with their origins at the DD diffraction points $Q_i (i = 1, 2)$, determined by standard ray tracing. Our description of the double diffraction mechanism is constructed directly in the TD as the superposition of two analogous mechanisms: a field diffracted from edge 2 when it is illuminated by the field diffracted from edge 1 (12), and that from 1 when it is illuminated by 2 (21). In the following, only the contribution 12 will be considered. The ray geometry for the field DD at Q_1 and Q_2 is depicted in Fig. 1 with ℓ the distance between the two diffraction points Q_1 and Q_2, and $\phi_{12}(\phi'_{12})$ the azimuthal coordinate of $Q_2\,(Q_1)$ measured in the system at edge 1 (2). TD and FD quantities are related by the Fourier transform pair

$$\psi(\omega) = \int_{-\infty}^{\infty} \hat{\psi}(t) e^{-j\omega t}\, dt \tag{2}$$

$$\hat{\psi}(t) = \frac{1}{2\pi} \int_{-\infty}^{\infty} \psi(\omega) e^{j\omega t}\, d\omega \tag{3}$$

and a caret $\hat{}$ tags time-dependent quantities. In order to permit spectral integration path deformations, it is convenient to introduce also the analytic transform [4]–[6].

$$\overset{+}{\psi}(t) = \frac{1}{\pi} \int_{0}^{\infty} \psi(\omega) e^{j\omega t}\, d\omega, \quad \text{with } \Im m\, t \geq 0. \tag{4}$$

The transform is analytic in the upper complex time plane. The physical transient field for t real is recovered by the limit on the real t axis $\hat{\psi}(t) = \Re e\, \overset{+}{\psi}(t)$.

A. Spectral Synthesis

Consider the first half plane illuminated by an impulsive spherical excitation $\delta(t - R_{P,P'}/c)/(4\pi R_{P,P'})$, with

$$R_{P(\phi_1),P'(\phi'_1)} = \big[r_1'^2 + r_1^2 + 2r_1 r'_1(\cos\beta'_1 \cos\beta_1 - \sin\beta'_1 \sin\beta_1 \cos(\phi_1 - \phi'_1))\big]^{1/2} \tag{5}$$

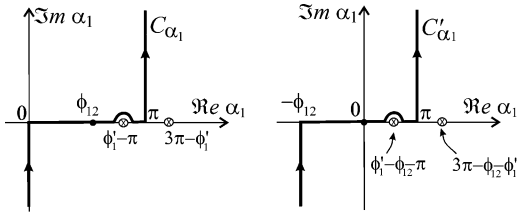

Fig. 3. Complex α_1 plane: Integration paths and their indentation with respect to the "incidence pole." In (b), the integration path C'_{α_1} and poles are shifted with respect to (a) by ϕ_{12}.

where $P'(\phi_1') \equiv (r_1', \pi - \beta_1', \phi_1')$ and $P(\phi_1) \equiv (r_1, \beta_1, \phi_1)$ are the source and observation locations, respectively, and c is the wave velocity in the medium. It is convenient to consider for the moment the analytic excitation $\overset{+}{\delta}(t - R_{P,P'}/c)/(4\pi R_{P,P'})$ with $\Im mt \geq 0$. We recall that

$$\overset{+}{\delta}\left(t - \frac{R_{P,P'}}{c}\right) = \frac{j}{\pi t} \quad \text{for } \Im mt > 0 \tag{6}$$

whereas

$$\delta\left(t - \frac{R_{P,P'}}{c}\right) = \Re e\ \overset{+}{\delta}\left(t - \frac{R_{P,P'}}{c}\right), \quad \text{for real time } t. \tag{7}$$

The TD response from the first edge to an impulsive spherical wave is obtained by the inverse Fourier transform of its FD counterpart, i.e., the FD-SD field by a half plane excited by a time harmonic spherical source [see [12] and (2)]

$$\psi_1^d(\omega) = \frac{1}{2\pi j}\int_{C_{\alpha_1}} \frac{e^{-jkR_{P(\phi_1),P'(\alpha_1+\pi)}}}{4\pi R_{P(\phi_1),P'(\alpha_1+\pi)}} G(\phi_1', \alpha_1)\, d\alpha_1 \tag{8}$$

with $k = \omega/c$ the free space wavenumber. The contour of integration C_{α_1} shown in Fig. 3(a) is defined along $(-j\infty, \pi + j\infty)$ for $\phi_1 < \pi$, whereas it must be defined along $(\pi - j\infty, 2\pi + j\infty)$ for $\phi_1 > \pi$. The spectral weight is

$$G(\phi', \phi) = -\frac{1}{2}\left[\sec\left(\frac{\phi' - \phi}{2}\right) \pm \sec\left(\frac{\phi' + \phi}{2}\right)\right] \tag{9}$$

with the upper/lower sign referring to hard/soft BC, and possesses "incidence" and "reflection" pole singularities as shown in Fig. 3(a). The integration path C_{α_1} is indented as in Figure in order to include/exclude the GO incident field residue contribution when the observation point at ϕ_1 is above/below the $\mathrm{SB}^{\mathrm{GO}}$ at $\phi_1 = \phi_1' - \pi$.

The TD-SD field from the first edge excited by the analytic waveform (6) is obtained from (4), and it is thus expressed as

$$\overset{+}{\psi}{}_1^d = \frac{1}{2\pi j}\int_{C_{\alpha_1}} \frac{\overset{+}{\delta}\left[t - R_{P(\phi_1),P'(\alpha_1+\pi)}/c\right]}{4\pi R_{P(\phi_1),P'(\alpha_1+\pi)}} G(\phi_1', \alpha_1) d\alpha_1. \tag{10}$$

The analytic delta (6) introduces a couple of time-dependent poles defined by the $\alpha_1(t)$ solutions of

$$ct - R_{P(\phi_1),P'(\alpha_1+\pi)} = 0. \tag{11}$$

It is important to note that the pole trajectories $\alpha_1(t)$, with varying time t, never cross the integration path (see Appendix A) so that no extra-field contribution due to the residue of a pole crossing the integration path must considered. The integral (10) is interpreted as a superposition of impulsive spectral sources $\overset{+}{\delta}[t - R_{P(\phi_1),P'(\alpha_1+\pi)}/c]/[4\pi R_{P(\phi_1),P'(\alpha_1+\pi)}]$, weighted by the spectral factor $G(\phi_1', \alpha_1)$, as shown in [12, Fig. 2]. Each spherical spectral source provides a diffracted field contribution from edge 2 at the observation point $P(\phi_2) \equiv (r_2, \beta_2, \phi_2)$, that is conveniently calculated using reciprocity, as the diffracted field from edge 2 at $P'(\alpha_1 + \pi)$ due to a point source at $P(\phi_2)$. Such contribution is represented as a summation of spectral spherical sources at $P(\alpha_2 + \pi)$ weighted by the spectral $G(\phi_2, \alpha_2)$, i.e.

$$\overset{+}{\psi}{}_2^d(\alpha_1) = \frac{1}{2\pi j}\int_{C_{\alpha_2}} \frac{\overset{+}{\delta}\left[t - R_{P'(\alpha_1+\pi),P(\alpha_2+\pi)}/c\right]}{4\pi R_{P'(\alpha_1+\pi),P(\alpha_2+\pi)}} \cdot G(\phi_2, \alpha_2) d\alpha_2 \tag{12}$$

in which $P(\alpha_2+\pi) \equiv (r_2, \pi - \beta_2, \alpha_2 + \pi)$, and the contour C_{α_2} has the same definition as C_{α_1}. Then, all the fields radiated by edge 2 (12) are superposed for each α_1-spectral spherical source in (10), i.e., $\overset{+}{\delta}[t - R_{P(\phi_1),P'(\alpha_1+\pi)}/c]/[4\pi R_{P(\phi_1),P'(\alpha_1+\pi)}]$ in (10) is replaced by $\overset{+}{\psi}{}_2^d(\alpha_1)$, leading to the double integral representation

$$\overset{+}{\psi}{}_{12}^{\mathrm{dd}} = \frac{-1}{4\pi^2}\int_{C_{\alpha_1}}\int_{C_{\alpha_2}} \frac{\overset{+}{\delta}\left[t - R(\alpha_1 - \phi_{12}, \alpha_2 - \phi_{12}')/c\right]}{4\pi R(\alpha_1 - \phi_{12}, \alpha_2 - \phi_{12}')} \cdot G(\phi_1', \alpha_1) G(\phi_2, \alpha_2) d\alpha_1 d\alpha_2. \tag{13}$$

In (13), $R(\alpha_1 - \phi_{12}, \alpha_2 - \phi_{12}') \equiv R_{P'(\alpha_1+\pi),P(\alpha_2+\pi)}$ is the distance between the spectral source and observation whose explicit expression is

$$\begin{aligned} R(\alpha_1, \alpha_2) &= [(r_1' + \ell + r_2)^2 + 2r_1'\ell g_1(\alpha_1) \\ &\quad + 2r_2\ell g_2(\alpha_2) + 2r_1'r_2 f(\alpha_1, \alpha_2)]^{1/2} \\ g_1(\alpha_1) &= \sin^2\beta_1'(\cos\alpha_1 - 1), \\ g_2(\alpha_2) &= \sin^2\beta_2(\cos\alpha_2 - 1) \\ f(\alpha_1, \alpha_2) &= g_1(\alpha_1) + g_2(\alpha_2) - \epsilon_{12}\sin\beta_1'\sin\beta_2 \\ &\quad \times [\cos(\beta_1' + \epsilon_{12}\beta_2)(\cos\alpha_1 - 1)(\cos\alpha_2 - 1) \\ &\quad + \sin\alpha_1\sin\alpha_2] \end{aligned} \tag{14}$$

with $\epsilon_{12} = \mathbf{u}_{\phi_{12}} \cdot \mathbf{u}_{\phi_{12}'}$ (note that $\epsilon_{12} = \pm 1$ being the unit vectors $\mathbf{u}_{\phi_{12}}$ and $\mathbf{u}_{\phi_{12}'}$ orthogonal to the plane containing the two edges). The introduction of the angles ϕ_{12} and ϕ_{12}', which *automatically appear* in our spectral synthesis, is convenient to parameterize the DD-field as a ray. In (13), $G(\phi_1', \alpha_1)$ and $G(\phi_2, \alpha_2)$ exhibit pole singularities that independently occur in the two variables of integration. Eventually, the change of variables $(\alpha_1 - \phi_{12}) \to \alpha_1$ and $(\alpha_2 - \phi_{12}') \to \alpha_2$ is performed, leading to

$$\overset{+}{\psi}{}_{12}^{\mathrm{dd}} = \frac{-1}{4\pi^2}\int_{C'_{\alpha_1}}\int_{C'_{\alpha_2}} \frac{\overset{+}{\delta}\left[t - R(\alpha_1, \alpha_2)/c\right]}{4\pi R(\alpha_1, \alpha_2)} \cdot G(\phi_1', \alpha_1 + \phi_{12}) G(\phi_2, \alpha_2 + \phi_{12}')\, d\alpha_1\, d\alpha_2 \tag{15}$$

in which the integration contours C'_{α_1} and C'_{α_2} are now translated and thus defined along $(-j\infty - \phi_{12}, \pi - \phi_{12} + j\infty)$ and $(-j\infty - \phi'_{12}, \pi - \phi'_{12} + j\infty)$, respectively. It is notable that our expression for the DD field (15) explicitly satisfies reciprocity. The term $R(\alpha_1, \alpha_2)/c$ is now be interpreted as a "spectral delay function" and it will play a dominant role in the wavefront approximation. The integrand in (15) presents various spectral singular points such as branch points, poles and "stationary delay" points (i.e., stationary points of the spectral delay function $R(\alpha_1, \alpha_2)/c$) in both variables that provide various localized wave mechanisms. For instance, residues in both variables at "optical" poles of the G functions provide GO (direct, reflected or doubly reflected) fields; pole in one variable and saddle point in the other provide edge SD fields that may have also undergone reflection at the other half-plane. The time-dependent (α_1, α_2)-poles introduced by the analytic delta are solution of the equation

$$ct - R(\alpha_1, \alpha_2) = 0 \tag{16}$$

and are discussed in Appendix A: it is shown that the trajectories of the poles in the α_1 plane for varying real t and α_2 on C'_{α_2}, never cross the integration path C'_{α_1}. A two-dimensional (2-D) stationary-delay point [i.e., stationary points of the spectral delay function $R(\alpha_1, \alpha_2)/c$, defined by $\nabla_{\alpha_1,\alpha_2} R(\alpha_1, \alpha_2) = 0$, at $(\alpha_1, \alpha_2) = (0,0)$] provides the DD ray. When the two edges are not parallel, other 2-D stationary-delay points are present that would provide spherical waves arising from the intersection of the two edges [20]. In the following, we will focus only on the wavefront approximation that will provide a uniform closed form result for the DD field.

III. Wavefront Approximations

The DD field in (15) is evaluated using a "wavefront approximation" based on the 2-D stationary delay point evaluation at $(\alpha_1, \alpha_2) = (0,0)$ that provides a good accuracy when the observer is located near the wavefront of the DD ray. In order to retain also a higher-order term in the wavefront approximation, and to uniformly take into account for the closeness of the poles to the stationary delay point, it is useful to split each G-spectral function in (15) in its even and odd parts

$$\begin{aligned} &G(\phi'_1, \alpha_1 + \phi_{12}) \\ &\quad = \mp\frac{1}{2}\sum_{p=1}^{2} \cdot \frac{(\pm 1)^p \sin\frac{\Phi_1^p}{2}\cos\frac{\alpha_1}{2} + (\mp 1)^p \cos\frac{\Phi_1^p}{2}\sin\frac{\alpha_1}{2}}{\cos^2\frac{\alpha_1}{2} - \cos^2\frac{\Phi_1^p}{2}} \\ &G(\phi_2, \alpha_2 + \phi'_{12}) \\ &\quad = \mp\frac{1}{2}\sum_{q=1}^{2} \cdot \frac{(\pm 1)^q \sin\frac{\Phi_2^q}{2}\cos\frac{\alpha_2}{2} + (\mp 1)^q \cos\frac{\Phi_2^q}{2}\sin\frac{\alpha_2}{2}}{\cos^2\frac{\alpha_2}{2} - \cos^2\frac{\Phi_2^q}{2}} \end{aligned} \tag{17}$$

where the upper/lower sign applies to hard/soft BC, and

$$\Phi_1^p = \phi'_1 + (-1)^p \phi_{12} + \pi, \quad (p = 1,2) \tag{18}$$

$$\Phi_2^q = \phi_2 + (-1)^q \phi'_{12} + \pi, \quad (q = 1,2). \tag{19}$$

Then, we introduce the change of variables $u = j\sin(\alpha_1/2)$, $v = j\sin(\alpha_2/2)$, and the GO-pole singularities of the two G functions in (17) are mapped onto $u = \pm j u_p$ and $v = \pm j v_q$, where $u_p = \sin(\Phi_1^p/2)$, and $v_q = \sin(\Phi_2^q/2)$. The value

$$\tau(u,v) \equiv R[\alpha_1(u), \alpha_2(v)]/c \tag{20}$$

represents the *arrival delay* of the u,v-spectral component. As shown in [5, sec. II-C.1], for the case of a single spectral integral, the wavefront approximations of the DD field is dominated by the value of the integrand at the stationary point of $\tau(u,v)$, defined as $\nabla_{uv}\tau(u,v) = 0$, that occurs at $(u,v) = (0,0)$ which is a minimum of the delay function $\tau(u,v)$. The spectral component there located dictates the DD field turn-on time

$$t^{\mathrm{dd}} \equiv \tau(0,0) = \frac{r'_1 + \ell + r_2}{c} \tag{21}$$

and the spectral components in its neighborhood build up constructively the early-time evolution of the DD field. As done in [12] for the FD case, a Taylor expansion of $\tau(u,v)$ up to second order around the stationary point gives

$$\tau(u,v) \approx t^{\mathrm{dd}} + \frac{1}{2}[\tau_{uu}u^2 + 2\tau_{uv}uv + \tau_{vv}v^2] \tag{22}$$

with $\tau_{uu} = 4\sin^2\beta'_1 r'_1(\ell + r_2)(r'_1 + \ell + r_2)^{-1}c^{-1}$, $\tau_{vv} = 4\sin^2\beta_2 r_2(r'_1 + \ell)(r'_1 + \ell + r_2)^{-1}c^{-1}$, and $\tau_{uv} = \epsilon_{12}\sin\beta'_1\sin\beta_2 r'_1 r_2(r'_1 + \ell + r_2)^{-1}c^{-1}$. The integration paths C'_u and C'_v, given by mapping the original contours C'_{α_1} and C'_{α_2} via the above change of variables, are now deformed onto the real u,v axes. In these deformations, pole singularities $\pm j u_p$, and $\pm j v_q$, obtained by mapping the "incidence" and "reflection" poles of the G functions (see Fig. 3), may be encountered. However their residue contributions are not considered here since they would give rise to standard GO or SD diffracted fields that are already accounted for *a priori* with their domains of existence (their SBs) determined by standard ray tracing.

The additional poles introduced by the analytic delta $\overset{+}{\delta}[t - \tau(u,v)]$ are defined by the solutions of

$$t - \tau(u,v) = 0 \tag{23}$$

shown in Fig. 13 before (a) and after (b) the path deformations in both variables u,v. Indeed, there the t-trajectories of the u-poles in the complex u plane are shown for v varying (a) along C'_v, and (b) along the real v-axis integration path. The pole trajectories in the v plane are analogous due to the symmetry of $\tau(u,v)$. In Appendix A it is illustrated how these TD-dependent poles are never captured in the path deformations in both variables. After all these manipulations, (15) is written as

$$\overset{+}{\psi}{}_{12}^{\mathrm{dd}}(t) = \sum_{p,q=1}^{2}\left[I^I_{pq} + I^{II}_{pq}\right] \tag{24}$$

with

$$I^I_{pq} = \int_{-\infty}^{\infty}\int_{\infty}^{\infty} B^I_{pq}(u,v)\frac{u_p v_q}{(u^2 + u_p^2)(v^2 + v_q^2)}\overset{+}{\delta}[t - \tau(u,v)]\,du\,dv \tag{25}$$

and

$$I_{pq}^{II}=\int_{\infty}^{\infty}\int_{\infty}^{\infty}B_{pq}^{II}(u,v)\frac{uv\overset{+}{\delta}[t-\tau(u,v)]}{\left(u^2+u_p^2\right)\left(v^2+v_q^2\right)}\,du\,dv. \quad (26)$$

The splitting of the original single spectral integral into (25) and (26) arises by multiplying the two even-even and odd-odd parts of the G-spectral functions in (17), whereas the resulting odd part of the integral vanishes. The two even functions in (25) and (26) are defined as

$$B_{pq}^{I}(u,v)=\frac{c(\pm1)^{p+q}}{16\pi^2\tau(u,v)} \quad (27)$$

$$B_{pq}^{II}(u,v)=-\frac{c(\mp1)^{p+q}}{16\pi^2\tau(u,v)}\frac{\sqrt{1-u_p^2}\sqrt{1-v_q^2}}{\sqrt{1+u^2}\sqrt{1+v^2}} \quad (28)$$

in which the upper/lower sign applies to hard/soft BC. As shown in Sections VI and VII, the terms I_{pq}^{II} are in general of higher order but render the final solution directly applicable to any double edge configuration, including the case when the two edges share a common face as in a strip or in a flat plate. Both B_{pq}^{I} and B_{pq}^{II} are regular slowly varying functions in a neighborhood of the stationary point $(u,v)=(0,0)$. Moreover, their gradients vanish at $(u,v)=(0,0)$ and in this neighborhood $B_{pq}^{I,II}(u,v)\approx B_{pq}^{I,II}(0,0)+Au^2+Buv+Cv^2+\cdots$, thus assuring that they can be evaluated at the stationary point and brought out of the integral with high accuracy.

In the sequel, a *nonuniform* evaluation for (25) and (26) is given first, that permits a ray-optical description of the TD-DD field but fails when both the SD and DD wavefronts arrive almost simultaneously at the observer location, i.e., when the pole singularities of the integrand occur close to or at the stationary point. Therefore, a *uniform* evaluation is also given that remains valid at any incidence/observation aspect describing the transitional behavior of the TD-DD field. The higher order terms u^2, uv, v^2 in I_{pq}^{I} are of the same asymptotic (wavefront) order as the dominant term in I_{pq}^{II} when $u_p, v_q\neq0$, but they are subdominant when $u_p=v_q=0$. Therefore, they are neglected since *only* the dominant term in I_{pq}^{II} may undergo a double transition when $u_p, v_q\to0$ (see Section VI-C).

After the quadratic approximation in the neighborhood of $(u,v)=(0,0)$, the spectral delay $\tau(u,v)$ in the argument of the analytic delta is purely real for all u,v on the real-axis integration paths. Therefore, in the following all the results are related to real time t simply using $\hat{\psi}(t)=\Re e\overset{+}{\psi}(t)$ and the property $\delta(t)=\Re e\overset{+}{\delta}(t)$, and all the above integrals, in particular (24)–(26), will provide the physical transient field $\hat{\psi}_{12}^{\rm dd}(t)$, as long as the analytic delta in (25), (26) is substituted by $\delta(t)$ with real time. Therefore, the DD field will be evaluated directly in closed form (see Appendixes B and C) and not by residue evaluations at the time dependent poles, as done in [5] and [9].

A. Nonuniform Wavefront Approximations

The nonuniform wavefront approximations for (25) and (26) are obtained evaluating $B_{pq}^{I,II}(u,v)/[(u^2+u_p^2)(v^2+v_q^2)]$ at the stationary phase point $(u,v)=(0,0)$, and the remaining double spectral integrals in closed form as in Appendix B. This leads to

$$I_{pq}^{I,nu}\sim B_{pq}^{I}(0,0)\frac{2\pi U(t-t^{\rm dd})}{u_pv_q\left(\tau_{uu}\tau_{vv}-\tau_{uv}^2\right)^{1/2}} \quad (29)$$

and

$$I_{pq}^{II,nu}\sim -B_{pq}^{II}(0,0)\frac{2\pi(t-t^{\rm dd})U(t-t^{\rm dd})\tau_{uv}}{u_p^2v_q^2\left(\tau_{uu}\tau_{vv}-\tau_{uv}^2\right)^{3/2}} \quad (30)$$

with $U(t)=0$ or 1 when $t<0$ or $t>0$, respectively. Combining all the p,q terms and substituting for u_p, v_q, τ_{uu}, τ_{vv}, τ_{uv}, leads to the compact representation for the TD-DD field

$$\hat{\psi}_{12}^{\rm dd}(t)\sim A^i(r_1')A(r_1',\ell,r_2)\hat{D}_{12}(t-t^{\rm dd}) \quad (31)$$

where

$$A^i(r_1')=\frac{1}{4\pi r_1'},\quad A(r_1',\ell,r_2)=\frac{\sqrt{r_1'}}{\sqrt{\ell r_2\left(r_1'+\ell+r_2\right)}} \quad (32)$$

are the incident spreading factor at Q_1 and the DD spreading factor, respectively. The *TD-DD coefficient* $\hat{D}_{12}(t)$ is evaluated at the retarded time $t-t^{\rm dd}$, where $t^{\rm dd}$ is the turn on time of the DD field defined in (21). As for the FD case [12], the splitting in (24) leads to a DD coefficient expressed by the sum

$$\hat{D}_{12}(t)=\hat{D}_{12}^{I}(t)+\hat{D}_{12}^{II}(t) \quad (33)$$

of a first and a second order *nonuniform TD-DD coefficients*

$$\hat{D}_{12}^{I}(t)=\frac{cU(t)}{8\pi\sin\beta_1'\sin\beta_2}\sum_{p,q=1}^{2}(\mp1)^{p+q}\frac{1}{\sin\frac{\Phi_1^p}{2}\sin\frac{\Phi_2^q}{2}} \quad (34)$$

$$\hat{D}_{12}^{II}(t)=\frac{-\epsilon_{12}c^2tU(t)}{32\pi\ell\sin^2\beta_1'\sin^2\beta_2}\times\sum_{p,q=1}^{2}(\pm1)^{p+q}\frac{\cos\frac{\Phi_1^p}{2}\cos\frac{\Phi_2^q}{2}}{\sin^2\frac{\Phi_1^p}{2}\sin^2\frac{\Phi_2^q}{2}} \quad (35)$$

with the upper (lower) sign referring to the soft (hard) BC.

B. Uniform Wavefront Approximations

The nonuniform wavefront approximation (31)–(35) for the DD field is singular for those incidence or observation aspects such that $\sin(\Phi_1^p/2)=0$ or $\sin(\Phi_2^q/2)=0$, respectively. The condition $\sin(\Phi_1^p/2)=0$ occurs when edge 2 is exactly either at the incidence $(p=1)$ or reflection $(p=2)$ SB due to edge 1 illuminated by the source at P'. Analogously, $\sin(\Phi_2^q/2)=0$ occurs when the observer at P is either at the incidence $(q=1)$ or reflection $(q=2)$ SB due to edge 2 when is illuminated by edge 1. These peculiar conditions are depicted in Figs. 4–6 where they are analyzed in detail. A *uniform* wavefront approximation which is well behaved at those aspects and compensates for the discontinuity of the edge-1 and edge-2 SD fields at their SBs (see Figs. 1 and 4–6) is derived uniformly accounting for the poles at $u=\pm ju_p$ and $v=\pm jv_q$ when evaluating (25) and (26), that may occur near or at the stationary delay point

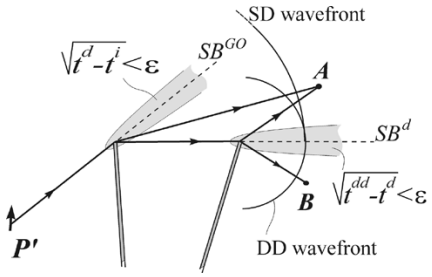

Fig. 4. SD and DD ray wavefronts and shadow boundaries (SB). Observer A is reached by both SD and DD fields, while B is reached only by the DD field. The SB^d plane bounds the domain of existence of the SD field. Conditions $\sqrt{t^{\mathrm{dd}} - t_1^d} < \epsilon$ and $\sqrt{t_1^d - t^i} < \epsilon$ define regions, with parabolic shape near the edges 2 and 1, respectively, where wavefronts arrive "almost" simultaneously.

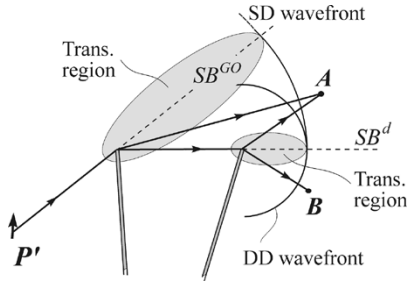

Fig. 5. TD transition regions (ellipses), SD and DD ray wavefronts and shadow boundaries (SB). The SB^d plane bounds the domain of existence of the SD field. The elliptical (if $\ell \gg r_2$) TD transition region defined by the *nondimensional* parameter $b_q/\sqrt{t - t^{\mathrm{dd}}} < \sigma$ is oriented along the SB^d. The vertex of the ellipse is at the DD wavefront.

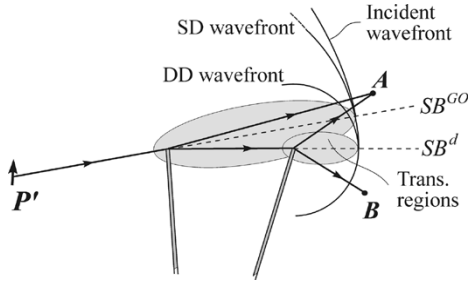

Fig. 6. Overlapping TD transition regions: the observer is reached by a transitional field diffracted at edge 2 that is illuminated itself by the transitional SD field at edge 1. Observer A will be reached by direct, SD and DD fields, while B will be reached only by the DD field. The SB^d plane bounds the domain of existence of the direct field, while the $\mathrm{SB}^{\mathrm{dd}}$ plane bounds the domain of existence of the transitional SD field. The three almost simultaneous wavefronts, direct, SD and DD, arrive at the observer A at instants t^i, t_1^d, and t^{dd}, respectively, with $t^i \leq t_1^d \leq t^{\mathrm{dd}}$.

$(u,v) = (0,0)$. To this end, the regular slowly varying parts $B_{pq}^{I,II}(u,v)$ in (25) and (26) are evaluated at $(u,v) = (0,0)$ (wavefront approximation) and the remaining integrals are expressed in a canonical form yielding

$$I_{pq}^{I} \sim I_{pq}^{I,nu} \hat{T}^{I}\left(\frac{a_p}{\sqrt{t - t^{\mathrm{dd}}}}, \frac{b_q}{\sqrt{t - t^{\mathrm{dd}}}}, w\right) \tag{36}$$

and

$$I_{pq}^{II} \sim I_{pq}^{II,nu} \hat{T}^{II}\left(\frac{a_p}{\sqrt{t - t^{\mathrm{dd}}}}, \frac{b_q}{\sqrt{t - t^{\mathrm{dd}}}}, w\right) \tag{37}$$

where we have introduced the *canonical transition functions*

$$\hat{T}^{I}\left(\frac{a}{\sqrt{t}}, \frac{b}{\sqrt{t}}, w\right) = \frac{a^2 b^2}{\pi(1-w^2)^{3/2}} \cdot \int_{-\infty}^{\infty}\int_{-\infty}^{\infty} \frac{\delta[t - (\xi^2 + 2w\xi\eta + \eta^2)]}{\left(\xi^2 + \frac{a^2}{1-w^2}\right)\left(\eta^2 + \frac{b^2}{1-w^2}\right)} d\xi\, d\eta \tag{38}$$

$$\hat{T}^{II}\left(\frac{a}{\sqrt{t}}, \frac{b}{\sqrt{t}}, w\right) = \frac{-2a^2 b^2}{\pi t w(1-w^2)^{1/2}} \cdot \int_{-\infty}^{\infty}\int_{-\infty}^{\infty} \xi\eta \frac{\delta[t - (\xi^2 + 2w\xi\eta + \eta^2)]}{\left(\xi^2 + \frac{a^2}{1-w^2}\right)\left(\eta^2 + \frac{b^2}{1-w^2}\right)} d\xi\, d\eta \tag{39}$$

with parameters

$$a_p = \sqrt{\frac{2}{c}}\sqrt{\frac{r_1'\ell}{r_1' + \ell}} \sin\beta_1' \sin\left(\frac{\Phi_1^p}{2}\right) \tag{40}$$

$$b_q = \sqrt{\frac{2}{c}}\sqrt{\frac{r_2\ell}{r_2 + \ell}} \sin\beta_2 \sin\left(\frac{\Phi_2^q}{2}\right) \tag{41}$$

and

$$w = \frac{\tau_{uv}}{\sqrt{\tau_{uu}\tau_{vv}}} = \frac{\sqrt{r_1' r_2}}{\sqrt{(r_1' + \ell)(r_2 + \ell)}}. \tag{42}$$

The normalization factors in front of (38) and (39) are chosen such that the uniform evaluation of (36) and (37) reduce to the nonuniform-ones when $\hat{T}^I \to U(t)$ and $\hat{T}^{II} \to U(t)$ [cfr. (58)]. Though the righthand sides of (38) and (39) appear to be a function of the four independent variables a, b, w, and t, a simple change of variables shows that they indeed depend only on the three independent parameters explicited in the respective left-hand sides. The TD transition functions (38) and (39) are evaluated in closed form in Appendix C as

$$\hat{T}^{I}(\hat{a}, \hat{b}, w) = \frac{U(t)}{\hat{c}^2 - 4w^2\hat{a}^2\hat{b}^2}\left[\frac{\hat{b}^2(\hat{c} - 2w^2\hat{a}^2)}{\sqrt{1 + \frac{1}{\hat{a}^2}}} + \frac{\hat{a}^2(\hat{c} - 2w^2\hat{b}^2)}{\sqrt{1 + \frac{1}{\hat{b}^2}}}\right] \tag{43}$$

$$\hat{T}^{II}(\hat{a}, \hat{b}, w) = \frac{2\hat{a}^2\hat{b}^2 U(t)}{\hat{c}^2 - 4w^2\hat{a}^2\hat{b}^2}\left[\frac{\hat{c} - 2\hat{b}^2}{\sqrt{1 + \frac{1}{\hat{a}^2}}} + \frac{\hat{c} - 2\hat{a}^2}{\sqrt{1 + \frac{1}{\hat{b}^2}}}\right] \tag{44}$$

with $\hat{c} = (1 - w^2) + \hat{a}^2 + \hat{b}^2$, and the total time dependence is taken into account by the *nondimensional* parameters $\hat{a}(t) = a/\sqrt{t}$ and $\hat{b}(t) = b/\sqrt{t}$.

1) Uniform TD-DD Coefficients: In summary, the TD-DD field is given by (31)–(33) with the *uniform* DD coefficients

$$\hat{D}_{12}^{I}(t) = \frac{cU(t)}{8\pi \sin\beta_1' \sin\beta_2} \sum_{p,q=1}^{2} (\mp 1)^{p+q} \cdot \frac{1}{\sin\frac{\Phi_1^p}{2} \sin\frac{\Phi_2^q}{2}} \hat{T}^{I}\left(\frac{a_p}{\sqrt{t}}, \frac{b_q}{\sqrt{t}}, w\right) \quad (45)$$

$$\hat{D}_{12}^{II}(t) = \frac{-\epsilon_{12} c^2 t U(t)}{32\pi \ell \sin^2\beta_1' \sin^2\beta_2} \sum_{p,q=1}^{2} (\pm 1)^{p+q} \cdot \frac{\cos\frac{\Phi_1^p}{2} \cos\frac{\Phi_2^q}{2}}{\sin^2\frac{\Phi_1^p}{2} \sin^2\frac{\Phi_2^q}{2}} \hat{T}^{II}\left(\frac{a_p}{\sqrt{t}}, \frac{b_q}{\sqrt{t}}, w\right) \quad (46)$$

that involve the TD-DD transition functions $\hat{T}^I$ and $\hat{T}^{II}$ parameterized in terms of the *nondimensional* parameters $a_p/\sqrt{t}$ and $b_q/\sqrt{t}$. Furthermore, we have explicited the unit step functions $U(t)$ to cast the *uniform* diffraction coefficients as a product between their *nonuniform* versions in (34) and (35), and the transition functions. Note that our wavefront approximations still preserve reciprocity.

IV. Direct TD Inversion From High-Frequency DD Fields

We show here that the uniform wavefront approximation for TD-DD field (31)–(33) with (45) and (46) coincides with the direct Fourier inversion of the uniform high-frequency expressions for the FD-DD field in [12] for time harmonic excitation. The FD-DD field ψ_{12}^{dd} arising from edge 2 upon illumination of diffracted field from edge 1, is [12]

$$\psi_{12}^{\mathrm{dd}} \sim A^i(r_1') A(r_1', \ell, r_2) e^{-jk(r_1'+\ell+r_2)} D_{12} \quad (47)$$

in which $A^i(r_1')e^{-jkr_1'}$ is the incident field at Q_1 on edge 1, $A(r_1', \ell, r_2)$ is the DD field spreading factor given in (32), and $k = \omega/c$ is the ambient wavenumber. The FD-DD coefficient is represented as $D_{12} = D_{12}^I + D_{12}^{II}$, where

$$D_{12}^{I} = \frac{1}{8\pi jk \sin\beta_1' \sin\beta_2} \sum_{p,q=1}^{2} (\mp 1)^{p+q} \cdot \frac{1}{\sin\frac{\Phi_1^p}{2} \sin\frac{\Phi_2^q}{2}} T^{I}(\sqrt{\omega}a_p, \sqrt{\omega}b_q, w) \quad (48)$$

and

$$D_{12}^{II} = \frac{-\epsilon_{12}}{32\pi k^2 \ell \sin^2\beta_1' \sin^2\beta_2} \sum_{p,q=1}^{2} (\pm 1)^{p+q} \cdot \frac{\cos\frac{\Phi_1^p}{2} \cos\frac{\Phi_2^q}{2}}{\sin^2\frac{\Phi_1^p}{2} \sin^2\frac{\Phi_2^q}{2}} T^{II}(\sqrt{\omega}a_p, \sqrt{\omega}b_q, w) \quad (49)$$

with FD-DD transition functions

$$T^{I}(\sqrt{\omega}a, \sqrt{\omega}b, w) = \frac{j\omega^2 a^2 b^2}{\pi(1-w^2)^{3/2}} \cdot \int_{-\infty}^{\infty}\int_{-\infty}^{\infty} \frac{e^{-j(\xi^2+2w\xi\eta+\eta^2)}}{\left(\xi^2 + \frac{\omega a^2}{1-w^2}\right)\left(\eta^2 + \frac{\omega b^2}{1-w^2}\right)} d\xi\, d\eta \quad (50)$$

$$T^{II}(\sqrt{\omega}a, \sqrt{\omega}b, w) = \frac{2\omega^2 a^2 b^2}{\pi w(1-w^2)^{1/2}} \cdot \int_{-\infty}^{\infty}\int_{-\infty}^{\infty} \frac{\xi\eta e^{-j(\xi^2+2w\xi\eta+\eta^2)}}{\left(\xi^2 + \frac{\omega a^2}{1-w^2}\right)\left(\eta^2 + \frac{\omega b^2}{1-w^2}\right)} d\xi\, d\eta. \quad (51)$$

In [12], T^I and T^{II} have been conveniently represented as combination of generalized Fresnel integrals [17], and computed easily as in [21]. However here, to determine the results for the inverse Fourier transform of ψ_{12}^{dd} we only need to transform $(j\omega)^{-1}T^I(a,b,w)$ and $(j\omega)^{-2}T^{II}(a,b,w)$. The parameters a_p, b_q of T^I and T^{II} in (48), (49) are all independent of ω and the normalization with respect to $\sqrt{\omega}$ has been made to prepare T^I and T^{II} for Fourier inversion. Performing the change of variables $\xi = \sqrt{\omega}\xi'$, $\eta = \sqrt{\omega}\eta'$, the exponential function becomes $\exp[-j\omega(\xi'^2 + 2w\xi'\eta' + \eta'^2)]$, all the ω disappear in the remaining part of the righthand side of (50), whereas in (51) one ω remains at the denominator, leading to

$$F^{-1}\left\{\frac{1}{j\omega} T^{I}(\sqrt{\omega}a_p, \sqrt{\omega}b_q, w)\right\} = \hat{T}^{I}\left(\frac{a_p}{\sqrt{t}}, \frac{b_q}{\sqrt{t}}, w\right) \quad (52)$$

$$F^{-1}\left\{\frac{-1}{\omega^2} T^{II}(\sqrt{\omega}a_p, \sqrt{\omega}b_q, w)\right\} = t\hat{T}^{II}\left(\frac{a_p}{\sqrt{t}}, \frac{b_q}{\sqrt{t}}, w\right) \quad (53)$$

in which $F^{-1}\{\ldots\}$ denotes inverse Fourier transform as in (3), and $\hat{T}^I$ and $\hat{T}^{II}$ are defined in (38) and (39), respectively. Since all the steps from (38), (39) to (43), (44) are exact, the inverse Fourier transform of the *uniform high-frequency result* ψ_{12}^{dd} is exactly the *uniform wavefront approximation* (31) with (45) and (46). Though this result would be straightforward for a *nonuniform* asymptotic/wavefront expansion, i.e., without transition functions, it is not for a *uniform* asymptotic/wavefront approximation. The key point is that the FD transition function is exactly related to the TD transition function as stated by (52) and (53), since the same decomposition of the weight spectral functions (15)–(28), and the same quadratic expansion (22) of the spectral delay $\tau(u,v)$ in the neighborhood of the stationary point $(u,v) = (0,0)$, have been adopted for both the FD and TD cases in [12] and here, respectively.

V. Electromagnetic DD Field

The solution for the scalar problem of skew edges with hard/soft BCs can be directly used to construct a solution for the vectorial problem of an electromagnetic arbitrarily polarized spherical wave illuminating a pair of skew edges with perfectly conducting faces. As done in [12], [14], [22]–[24] for the double diffraction problem and in [25] for the single diffraction problem, the scalar solutions for hard and soft BCs are used to construct a compact diagonal dyadic DD coefficient in the ray fixed reference systems. To this end, at the two diffraction points Q_1 and Q_2 (see Fig. 2) the ray fixed coordinate systems are defined through the unit vectors $(\mathbf{u}_{r_1'}, \mathbf{u}_{\beta_1'}, \mathbf{u}_{\phi_1'})$ from the source P' to Q_1, and $(\mathbf{u}_{r_2}, \mathbf{u}_{\beta_2}, \mathbf{u}_{\phi_2})$ from Q_2 to the observation point P. Ray fixed coordinate systems connecting edge 1 and 2 are not necessary since the two edges are coplanar and the interaction between the two edges does not cause depolarization for the leading asymptotic terms treated in this paper. The

arbitrarily polarized impulsive incident wave at Q_1 is denoted as $\hat{\mathbf{E}}^i(Q_1) = \mathbf{E}_0^i \delta(t - r_1'/c) A^i(r_1')$, where the arbitrary polarization factor expressed in the incident ray fixed coordinate system is denoted by $\mathbf{E}_0^i(Q_1) \equiv E^i_{\beta_1'} \mathbf{u}_{\beta_1'} + E^i_{\phi_1'} \mathbf{u}_{\phi_1'}$. The DD electric field mechanism 12 evaluated at the observation point P is denoted by

$$\hat{\mathbf{E}}_{12}^{\mathrm{dd}}(t) \equiv \hat{E}^{\mathrm{dd}}_{\beta_2}(t) \mathbf{u}_{\beta_2} + \hat{E}^{\mathrm{dd}}_{\phi_2}(t) \mathbf{u}_{\phi_2} \tag{54}$$

and is given by

$$\hat{\mathbf{E}}_{12}^{\mathrm{dd}}(t) \sim \mathbf{E}_0^i A^i(r_1') A(r_1', \ell, r_2) \underline{\hat{\mathbf{D}}}_{12}(t - t^{\mathrm{dd}}) \tag{55}$$

where $A^i(r_1')$ is the incident spreading factor in (32), $A(r_1', \ell, r_2)$ is the DD spreading factor in (32), t^{dd} is the retarded time in (21) and the dyadic TD-DD coefficient is represented as

$$\underline{\hat{\mathbf{D}}}_{12}(t) = \epsilon_{12} \left(\mathbf{u}_{\beta_1'} \mathbf{u}_{\beta_2} \hat{D}^s_{12}(t) + \mathbf{u}_{\phi_1'} \mathbf{u}_{\phi_2} \hat{D}^h_{12}(t) \right) \tag{56}$$

where $\hat{D}^{s,h}_{12}(t)$ are the scalar soft and hard TD-DD coefficients in (33) with (45) and (46). The dyad includes a leading order term (45), and a higher order term (46) that however is important in single and double transition regions to recover the main phenomenology of electromagnetic scattered fields.

VI. Phenomenology and Discussion

The uniform wavefront approximation for the DD field $\hat{\psi}^{\mathrm{dd}}_{12}$ in (31)–(33) consists of two terms associated to $\hat{D}^I_{12}(t - t^{\mathrm{dd}})$ and $\hat{D}^{II}_{12}(t - t^{\mathrm{dd}})$ in (45) and (46). Accordingly, it will be convenient to split the DD field as

$$\hat{\psi}^{\mathrm{dd}}_{12}(t) = \hat{\psi}^{\mathrm{dd},I}_{12}(t) + \hat{\psi}^{\mathrm{dd},II}_{12}(t). \tag{57}$$

Their phenomenology is governed by the *nondimensional* parameters $a_p/\sqrt{t - t^{\mathrm{dd}}}$ and $b_q/\sqrt{t - t^{\mathrm{dd}}}$. In the following, we highlight wave phenomenologies related to various locations of the observation point P. Similar concepts (not shown for space limitation) also apply for incident aspects, i.e., to P', since the TD-DD field here derived fully satisfies reciprocity.

A. TD-DD Field at Its Wavefront

At the wavefront of a DD ray, shown in Fig. 4, the uniform DD coefficient $\hat{D}_{12}$ in (31) is evaluated for $t \approx t^{\mathrm{dd}}$. Thus, $|a_p|/\sqrt{t - t^{\mathrm{dd}}} \to \infty$ and $|b_q|/\sqrt{t - t^{\mathrm{dd}}} \to \infty$, whence the transition functions $\hat{T}^I$ and $\hat{T}^{II}$ in (45) and (46) are approximated for large first two parameters as

$$\hat{T}^I(\infty, \infty, w) \to 1, \quad \hat{T}^{II}(\infty, \infty, w) \to 1 \tag{58}$$

and the uniform DD coefficients (45), (46) reduce to their nonuniform versions (34) and (35). It is worth noting that *at* the DD wavefront, (58) still holds in the proximity of the SB of SD rays, e.g., SB^d in Fig. 4. In the FD, the transition region around SB^d is bounded by a parabola when $r_2 \ll \ell$ (the shape is obtained imposing the parameter $|b_q| < \epsilon$, being ϵ an assigned small quantity) as shown by the grey region in Fig. 4 for $q = 1$. In the TD, the FD transition region collects all the observation points where SD and DD wavefronts arrive almost simultaneously, i.e., where $\sqrt{t^{\mathrm{dd}} - t_1^d} \approx |b_1| < \epsilon$, with $t_1^d = (r_1^{d\prime} + r_1^d)/c$ the turn-on time of the SD ray diffracted at edge 1, being $r_1^{d\prime}(r_1^d)$ the distance between $P'(P)$ and the diffraction point of the SD ray. Conversely, TD-DD transition regions are defined as the regions where the transition functions $\hat{T}^I$ and $\hat{T}^{II}$ differ significantly from unity, i.e., where their nondimensional argument $|b_q|/\sqrt{t - t^{\mathrm{dd}}} < \sigma$, being σ a sufficiently small number. As shown in Fig. 5 for $q = 1$, when $r_2 \ll \ell$ the TD transition region has an elliptical shape whose size grows with time t. The evolving TD-DD transition regions are tangent to the moving DD wavefront.

B. TD-DD Field Behind Its Wavefront

Behind the wavefront, the arguments of the transition functions in (45) and (46) decrease, and the TD-DD transition region in Fig. 5 becomes larger and larger remaining tangent the the moving DD wavefront. Eventually, for $t \to \infty$, $|\hat{a}_p| = |a_p|/\sqrt{t - t^{\mathrm{dd}}} \to 0$ and $|\hat{b}_q| = |b_q|/\sqrt{t - t^{\mathrm{dd}}} \to 0$, and the transition functions $\hat{T}^I$ and $\hat{T}^{II}$ vanish providing a smooth transition from the early time to a late-time decaying response.

The uniform wavefront approximation for the TD-DD field is not expected to be accurate for late time instants since it is obtained expanding the argument of the delta Dirac function around the spectral components $(u, v) = (0, 0)$ which define the ray field (usually referred to as *wavefront approximation*). Equivalently, the TD-DD field is also obtained inverting from the FD the high-frequency expressions for DD field (see Section IV); hence a convolution with an excitation waveform dominated by high frequencies, whose frequency spectrum has no low-frequency components, may enlarge the range of validity of the resulting pulsed response to later observation times.

C. Shadow Boundary Limits

It is well-known that the GO field is spatially discontinuous at its incidence and reflection SBs (see Figs. 4 and 5 where the incidence $\mathrm{SB}^{\mathrm{GO}}$ is shown) and the SD field compensates for those discontinuities undergoing a transitional behavior [7]–[9], [11], [25]. In our double edge configuration, the SD field at edge 1 is optically shadowed by edge 2 at its SB^d (see Fig. 5). We analyze here the transitional behavior of the DD field $\hat{\psi}^{\mathrm{dd},I}_{12}(t)$ in two distinct configurations, when the SD field experience a ray optical shadowing at its SB^d (Fig. 5), and when the GO and SD fields experience optical shadowing at their almost overlapped $\mathrm{SB}^{\mathrm{GO}}$ and SB^d (Fig. 6). In the latter case the shadowed SD field is in its transition requiring a *double transition* of the DD field.

1) Observer or Source in Transition Region: We first consider the case when the observation point crosses the plane containing edges 1 and 2, depicted in Figs. 4 and 5. There, the SD field from edge 1 is spatially discontinuous at and behind its wavefront (i.e., for $t \geq t_1^d$), due to the shadowing by edge 2. At this aspect, $\phi_2 = \phi_{12}' + \pi$, so that $\Phi_2^1 = 2\pi$ and consequently $b_1 = 0$ (see [12]), implying that $t^{\mathrm{dd}} = t_1^d$, i.e., the SD and DD wavefronts arrive simultaneously. Therefore, approaching

the SB^d depicted in Fig. 5, both $q = 1$ terms in (45), (46) experience a transitional behavior because the TD-DD transition functions there reduce to

$$\hat{T}^I(\hat{a}, \hat{b} \to 0, w) = |\hat{b}| \frac{\hat{a}^2}{1 - w^2 + \hat{a}^2}, \tag{59}$$

$$\hat{T}^{II}(\hat{a}, \hat{b} \to 0, w) = \hat{b}^2 \frac{2|\hat{a}|^3}{[1 - w^2 + \hat{a}^2]\sqrt{1 + \hat{a}^2}}. \tag{60}$$

After their insertion in (45) and (46) and (31), the DD field $\hat{\psi}_{12}^{\mathrm{dd},I}$ reduces to

$$\hat{\psi}_{12}^{\mathrm{dd},I}(t) = -\frac{1}{2}\mathrm{sgn}(b_1)\hat{\psi}_1^d(t) + \hat{g}(t)U(t - t^{\mathrm{dd}}) \tag{61}$$

where

$$\hat{\psi}_1^d(t) = A^i(r_1') \frac{\sqrt{r_1'}}{\sqrt{r_1(r_1' + r_1)}} \frac{\sqrt{c}U(t - t_1^d)}{4\pi \sin\beta_1' \sqrt{2(t - t_1^d)}} \cdot \sum_{p=1}^{2} \frac{(\mp 1)^{p+1}}{\sin\frac{\Phi_1^p}{2}} \frac{a_p^2}{(1 - w^2)(t - t_1^d) + a_p^2} \tag{62}$$

is the TD-UTD SD field [11] singular at the wavefront $t = t_1^d$. The other field contribution $\hat{g}(t)U(t - t^{\mathrm{dd}})$ in (61), as well as $\hat{\psi}_{12}^{\mathrm{dd},II}$, are higher order terms that behave like a step function $U(t - t^{\mathrm{dd}})$, and are spatially continuous across the SB^d line at and behind the wavefront. Thus, $\hat{\psi}_{12}^{\mathrm{dd}}$ compensates for the discontinuity of $\hat{\psi}_1^d$ at the $\mathrm{SB}^d \phi_2 = \phi_{12}' + \pi$, at and behind the wavefront, recovering the well-known $1/\sqrt{t}$ time dependence of the SD field.

Conversely, when the source crosses the plane containing the edges causing edge 2 to be in the shadow (lit) region of the incident field, the SD field $\hat{\psi}_2^d$ abruptly disappears (appears). At this aspect, $\phi_1' = \phi_{12} + \pi$, so that $\Phi_1^1 = 2\pi$ and consequently $a_1 = 0$ (see [12]). Again, reciprocally to the previous case, the DD field $\hat{\psi}_{12}^{\mathrm{dd}}$ is in transition and restores the continuity of the total field for varying incident aspect. Similar considerations apply to discontinuities for $a_2 = 0$ and $b_2 = 0$, caused by shadowed reflected-diffracted and diffracted-reflected mechanisms, respectively.

2) Double Transition Region: When *both* source and observer lie on the plane containing the two edges, all the arrival times of the incident, SD and DD wavefronts coincide, i.e., $t^{\mathrm{dd}} = t_1^d = t^i$, where $t^i = |P - P'|/c$ is the arrival time of the incident field. At this peculiar incident-observation aspect $a_1 = b_1 = 0$, hence immediately *behind* the DD wavefront $\hat{a}_1 = a_1/\sqrt{t - t^{\mathrm{dd}}} = 0$, $\hat{b}_1 = b_1/\sqrt{t - t^{\mathrm{dd}}} = 0$ and the TD-DD transition functions vanish as

$$\hat{T}^I(\hat{a} \to 0, \hat{b} \to 0, w) = \frac{|\hat{a}\hat{b}|(|\hat{a}| + |\hat{b}|)}{1 - w^2} \tag{63}$$

$$\hat{T}^{II}(\hat{a} \to 0, \hat{b} \to 0, w) = \frac{(\hat{a}\hat{b})^2(|\hat{a}| + |\hat{b}|)}{1 - w^2}. \tag{64}$$

As can be inferred substituting (63) and (64) in (45) and (46), the $p = q = 1$ terms in $\hat{\psi}_{12}^{\mathrm{dd},I}(t)$ and $\hat{\psi}_{12}^{\mathrm{dd},II}(t)$ vanish for every $t \neq t^{\mathrm{dd}} \equiv t^i$. In order to understand the double transition behavior *at* the wavefront, we consider an observer tied to the DD wavefront, with both source and observer in proximity of (and not at) the plane containing the two edges. In this double transition, $\mathrm{SB}^{\mathrm{GO}}$ is close to SB^d, consequently the arrival times of the incident, SD and DD fields *almost* coincide and the parameters a_1 and b_1 are small but not vanishing. Exactly at the DD wavefront $t = t^{\mathrm{dd}} \approx t^i$, the two nondimensional parameters $\hat{a}_1 = a_1/\sqrt{t - t^{\mathrm{dd}}} = \infty$, $\hat{b}_1 = b_1/\sqrt{t - t^{\mathrm{dd}}} = \infty$, and the two transition functions equal one as shown in (58). As a consequence, at the DD wavefront, when both source and observer approach the plane containing the two edges, both $a_1, b_1 \to 0$, and the $p = q = 1$ terms in $\hat{\psi}_{12}^{\mathrm{dd},I}(t)$ and $\hat{\psi}_{12}^{\mathrm{dd},II}(t)$ experience a singularity. In summary, in this double transition limit the $p = q = 1$ terms have a delta Dirac impulsive behavior $\delta(t - t^i)$ at the DD wavefront. Their weights are determined by time-integrating the $p = q = 1$ terms of $\hat{\psi}_{12}^{\mathrm{dd},I}(t)$ and $\hat{\psi}_{12}^{\mathrm{dd},II}(t)$ prior to the limit $a_1, b_1 \to 0$. Using a decomposition of (43) and (44) in simple terms, and the formula $\int_1^\infty [(a + x)\sqrt{x}]^{-1} dx = (2\arctan\sqrt{a})/\sqrt{a}$, one obtains

$$\int_0^\infty \hat{T}^I(a/\sqrt{t}, b/\sqrt{t}, w)\, dt = \pi|ab|/\sqrt{1 - w^2} \tag{65}$$

and

$$\int_0^\infty t\hat{T}^{II}(a/\sqrt{t}, b/\sqrt{t}, w)\, dt = 4\pi(ab)^2 \arcsin(w)/(w\sqrt{1 - w^2}). \tag{66}$$

Finally, performing the limit $a_1, b_1 \to 0$, leads to the double transition limit of the DD fields

$$\hat{\psi}_{12}^{\mathrm{dd},I} = \frac{1}{4}\mathrm{sgn}(a_1 b_1) \frac{\delta(t - t^i)}{4\pi|P - P'|}, + \hat{g}^I(t)U(t - t^i) \tag{67}$$

$$\hat{\psi}_{12}^{\mathrm{dd},II} = \frac{\arcsin(w)}{2\pi} \frac{\delta(t - t^i)}{4\pi|P - P'|} + \hat{g}^{II}(t)U(t - t^i). \tag{68}$$

The field $\hat{\psi}_{12}^{\mathrm{dd},I}$ reduces to a quarter of the GO field (i.e., the free-space spherical illuminating impulse). The sign function permits to restore the continuity of the total field on the SB^d at and after the wavefronts. The higher order DD field $\hat{\psi}_{12}^{\mathrm{dd},II}$, at this double transition limit, is a delta Dirac impulse like $\hat{\psi}_{12}^{\mathrm{dd},I}$ and the incident field. Though it does not contribute to repair the discontinuity introduced by the appearance/disappearance of the incident and SD fields, its contribution is fundamental to achieve an accurate prediction of the DD response in this double transition region (see [26]–[28] for a FD description). Furthermore, it may be the only existing contribution in particular cases such as the one in the sequel. Similar considerations apply when reflected or doubly reflected GO SBs and reflected-diffracted or diffracted-reflected SBs overlap.

VII. DD Field at a Flat Plate

The DD field scattered by two edges of a flat plate shown in Fig. 7 can be seen as a particular case of the general solution (31) when the two edges share a common face. In this case $\phi_{12}' =$

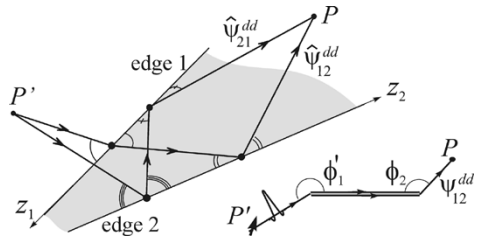

Fig. 7. Flat plate. The two DD mechanisms $\hat{\psi}_{12}$ and $\hat{\psi}_{21}$ are shown.

$\phi_{12} = 0$, as a consequence $\Phi_1^1 = \Phi_1^2 = \phi_1' + \pi$ and $\Phi_2^1 = \Phi_2^2 = \phi_2 + \pi$, and the parameters in (41) reduce to $a_1 = a_2 = a$ and $b_1 = b_2 = b$, with

$$a = \sqrt{2/c}\sin\beta_1'\sqrt{r_1'\ell/(r_1'+\ell)}\cos(\phi_1'/2) \tag{69}$$

$$b = \sqrt{2/c}\sin\beta_2\sqrt{r_2\ell/(r_2+\ell)}\cos(\phi_2/2). \tag{70}$$

Therefore, the four terms in the p,q-sum in (45) and (46) coincide, implying that for *soft* BC $\hat{D}_{12}^{I,s}(t) = 0$ and

$$\hat{D}_{12}^{s}(t) = \hat{D}_{12}^{II,s}(t) = \frac{-\epsilon_{12}c^2 tU(t)}{8\pi\ell\sin^2\beta_1'\sin^2\beta_2} \cdot \frac{\sin\frac{\phi_1'}{2}\sin\frac{\phi_2}{2}}{\cos^2\frac{\phi_1'}{2}\cos^2\frac{\phi_2}{2}} T^{II}\left(\frac{a}{\sqrt{t}}, \frac{b}{\sqrt{t}}, w\right) \tag{71}$$

whereas for hard BC, $\hat{D}_{12}^{II,h}(t) = 0$ and

$$\hat{D}_{12}^{h}(t) = \hat{D}_{12}^{I,h}(t) = \frac{cU(t)}{2\pi\sin\beta_1'\sin\beta_2} \cdot \frac{1}{\cos\frac{\phi_1'}{2}\cos\frac{\phi_2}{2}} \hat{T}^{I}\left(\frac{a}{\sqrt{t}}, \frac{b}{\sqrt{t}}, w\right). \tag{72}$$

The phenomenology outlined in Sections VI-A and VI-B still applies to this particular case. At the wavefront $t = t^{\mathrm{dd}}$, or out of transition regions, $\hat{T}^I \to 1$ and $\hat{T}^{II} \to 1$, and the uniform wavefront approximations (71), (72) coincide with the nonuniform ones. Our nonuniform TD-DD result [(31) with (71) and (72), assuming $\hat{T}^I = \hat{T}^{II} = 1$] applied to the conducting strip problem (two parallel edges) is coincident with the wavefront approximation of the second order diffraction mechanisms obtained in ([18], (5)–(6)), and [19] for both hard and soft cases and plane wave excitation. This has been obtained reducing our result (31) to unit amplitude plane wave excitation via the limit $A(r_1' \to \infty, \ell, r_2) \to 1/\sqrt{\ell r_2}$ and $A^i = 1$, and considering orthogonal incidence $(\beta_1' = \beta_2 = \pi/2)$ in (71) and (72).

VIII. Numerical Examples

The compensation and transitional behavior discussed in Section VI-C is here investigated numerically for a particular geometry determined by $r_1' = 42$ cm; $\ell = 45$ cm; $r_2 = 33$ cm; $\beta_1' = 100°$; $\beta_2 = 50°$; $\phi_{12}' = 100°$; $\phi_{12} = 100°$ (see Fig. 2). The source at P' radiates a spherical pulse $\hat{s}(t - |P - P'|/c)/(4\pi|P - P'|)$. If the incident field pulse $\hat{s}(t)$ is band limited, the DD band limited response $\hat{\psi}^{\mathrm{dd,BL}}(t)$ is obtained by the time convolution

$$\hat{\psi}^{\mathrm{dd,BL}}(t) = \hat{s}(t) * \hat{\psi}^{\mathrm{dd}}(t) \tag{73}$$

with the impulsive response $\hat{\psi}^{\mathrm{dd}}(t)$ in (31).

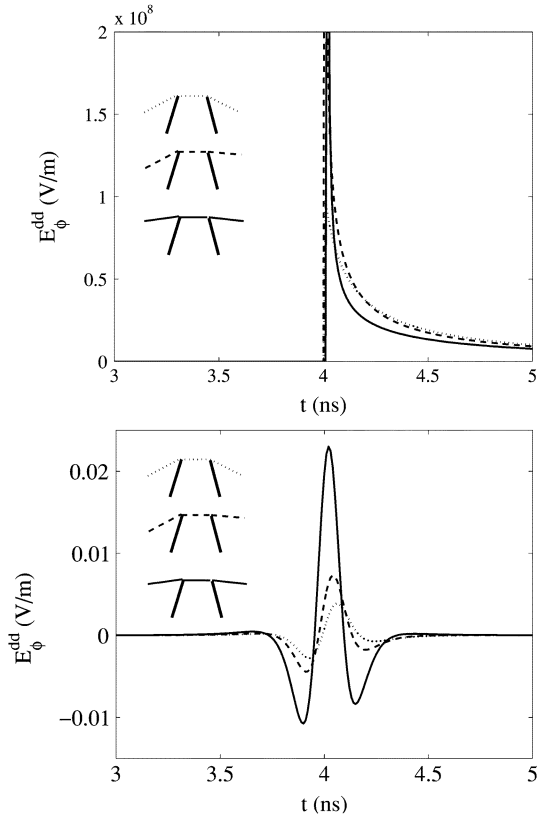

Fig. 8. TD-DD field $\hat{\psi}_{12}^{\mathrm{dd}}$ with (a) impulsive excitation; (b) band limited excitation: normalized Rayleigh pulse $\hat{G}(t) = \Re e[j/(j + 2\pi f_M t/4)^5]$; central frequency $f_M = 3$ GHz ($\lambda_M = c/f_M = 10$ cm). Geometry: $r_1' = 42$ cm; $\ell = 45$ cm; $r_2 = 33$ cm; $\beta_1' = 100°$; $\beta_2 = 50°$; $\phi_{12}' = 100°$; $\phi_{12} = 100°$, hard BC. In both cases (a) and (b), three distinct wave regimes are analyzed as shown in the inset. Dotted line: far from transition regions $(\phi_1' = 310°, \phi_2 = 310°)$. Dashed line: observer in transition region $(\phi_1' = 310°, \phi_2 = 281° \approx \phi_{12}' + 180°)$. Continuous line: source and observer both in transition region $(\phi_1' = 281°, \phi_2 = 281°)$.

In Fig. 8 we analyze a scalar case with hard BC. In Fig. 8(a) the excitation waveform is a Dirac delta function $\hat{s}(t) = \delta(t)$, whereas in Fig. 8(b) the excitation waveform is a normalized Rayleigh pulse $\hat{s}(t) = \Re e[j/(j + 2\pi f_M t/4)^5]$, whose spectrum $s(\omega) = \pi(6\omega_M)^{-1}(4\omega/\omega_M)^4 e^{-4|\omega|/\omega_M}$ has a central frequency $f_M = \omega_M/(2\pi) = 3$ GHz, corresponding to a central wavelength $\lambda_M = c/f_M = 10$ cm. In both cases (a) and (b), three distinct wave regimes are analyzed as shown in the insets. Dotted line: far from transition regions $(\phi_1' = 310°, \phi_2 = 310°)$. Dashed line: observer in transition region $(\phi_1' = 310°, \phi_2 = 281° \approx \phi_{12}' + 180°)$. Continuous line: source and observer both in transition regions (double transition) $(\phi_1' = 281°, \phi_2 = 281°)$. For delta excitation the transitional behavior is not so apparent in Fig. 8(a), but it is clearly shown in Fig. 8(b) for band limited excitation. There, the TD-DD field out of transition (dotted line) is shaped as the primitive of the exciting Rayleigh pulse, in accordance with the $1/\omega$-frequency dependence of the FD-DD field [e.g. (48)].

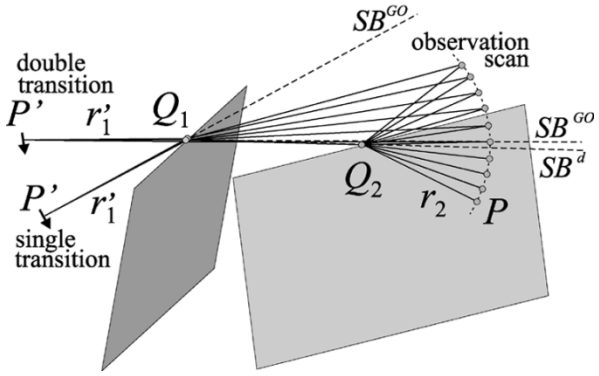

Fig. 9. Double edge geometry for the field evaluations in Figs. 10 and 11, along the angular scan centered at Q_2. Constant parameters: $r_1' = 42$ cm; $\ell = 45$ cm; $r_2 = 33$ cm; $\beta_1' = 100°$; $\beta_2 = 50°$; $\phi_{12}' = 100°$; $\phi_{12} = 100°$. Varying parameter: ϕ_2 ranging from 225° to 315°, i.e., $\pm 45°$ across the SB^d at $\phi_2 = 280°$. Two distinct source locations are considered: in Fig. 10, $\phi_1' = 310°$ and the $\mathrm{SB}^{\mathrm{GO}}$ is off the angular scan; in Fig. 11, $\phi_1' = 281°$ and the $\mathrm{SB}^{\mathrm{GO}}$ at $\phi_2 = 278°$ is close to the SB^d. In both cases the source is an electric dipole oriented along $\mathbf{u}_{\beta_1'}$ radiating a normalized Rayleigh pulse $\hat{G}(t) = \Re e[j/(j + 2\pi f_M t/4)^5]$ with central frequency $f_M = 3$ GHz.

When the source is in transition region (dashed line) the DD field is shaped like a SD field [see (61)], whereas when both source and observer are in transition regions (double transition) the waveform of the TD-DD field recovers that of the incident field as demonstrated analytically in (67).

Along the observation scan in Fig. 9, the space-time behavior of the spatially discontinuous standard GO + SD $\hat{\psi}^{\mathrm{GO}}(t) + \hat{\psi}_1^d(t)$ and DD $\hat{\psi}_{12}^{\mathrm{dd}}(t)$ fields, and of the continuous total field $\hat{\psi}^{\mathrm{GO}}(t) + \hat{\psi}_1^d(t) + \hat{\psi}_{12}^{\mathrm{dd}}(t)$, are described for an observer that undergoes a single (Fig. 10) and double (Fig. 11) transition, respectively. In both cases, the same geometry and the same band limited source excitation $\hat{s}(t)$ as in the previous case are considered, though we have dropped the superscript BL for simplicty. Field contributions are plotted against time and observation angle ϕ_2. Existence of the GO field is limited by the $\mathrm{SB}^{\mathrm{GO}}$, whereas the SD field is bounded by the SB^d at $\phi_2 = \phi_2' + 180° = 280°$, causing abrupt spatial discontinuities.

In Fig. 10, the source is located at $\phi_1' = 310°$ implying that the $\mathrm{SB}^{\mathrm{GO}}$ and SB^d are far apart as in Fig. 5. Therefore, the SD field $\hat{\psi}_1^d(t)$ is out of transition when abruptly disappears at the SB^d [Fig. 10(a)]. The DD field $\hat{\psi}_{12}^{\mathrm{dd}}(t)$ exhibits an opposite discontinuity [Fig. 10(b)], to restore the continuity of the total field in Fig. 10(c), at any point and any time.

In Fig. 11, the same space-time aspects are analyzed as in Fig. 10. The only difference is that the source is at $\phi_1' = 281°$, and the SD field is in its transition (ready to compensate for the GO field discontinuity at the $\mathrm{SB}^{\mathrm{GO}}$) at its SB^d. Indeed, as explained in Fig. 6, $\mathrm{SB}^{\mathrm{GO}}$ at $\phi_2 \approx 278°$ and SB^d at $\phi_2 = 280°$ almost overlap. Therefore, the strong discontinuity of the transitional SD field $\hat{\psi}_1^d(t)$ at its SB^d (note the different scales in Figs. 10 and 11) is compensated by an opposite discontinuity of the DD field $\hat{\psi}_{12}^{\mathrm{dd}}(t)$ [Fig. 11(b)], that there experiences a double transition. The total field in Fig. 11(c) is continuous at any point and any time.

Note that for increasing observation angle ϕ_2, passing from the lit to the shadow region, the total TD field waveform in Figs. 10(c) and 11(c) gradually weakens and transforms, according to the presence of the only higher order mechanism in the shadow region.

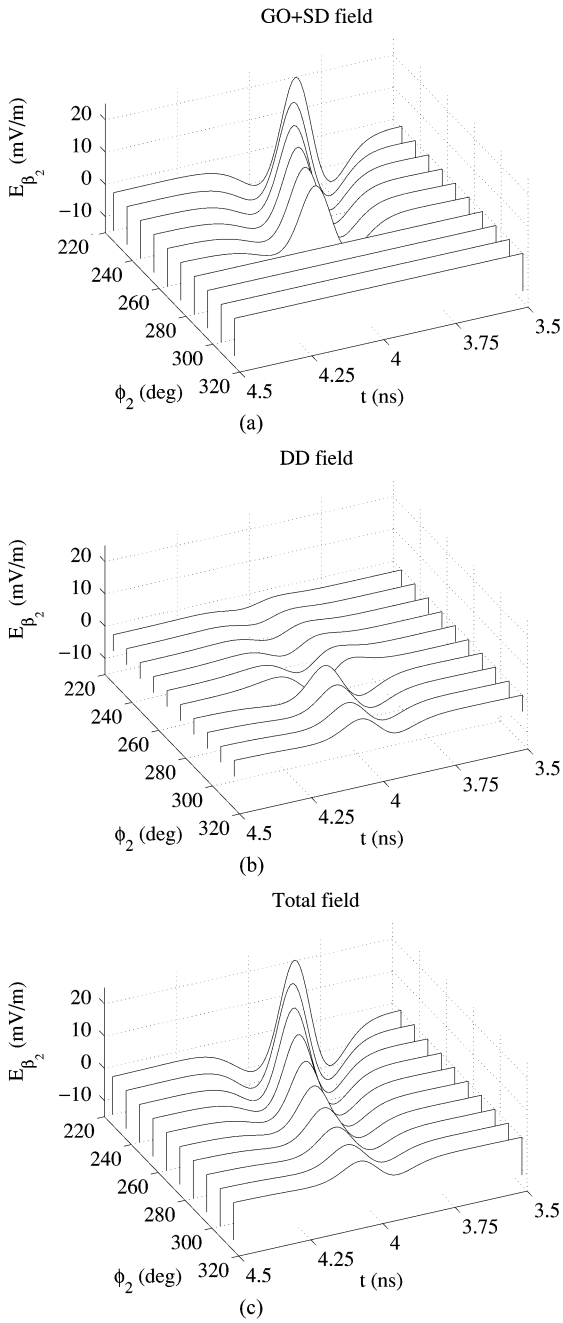

Fig. 10. $\mathbf{u}_{\beta_2}$ component of the transient electric field is plotted along the observation scan in Fig. 9 varying the observation angle ϕ_2. The source dipole is at $\phi_1' = 310°$ (single transition case) and oriented along $\mathbf{u}_{\beta_1'}$, all the geometry and source parameters are shown in Fig. 9. In (a), the standard GO + SD transient field abruptly vanishes beyond the SB^d at $\phi_2 = 280°$. In (b), the TD-DD field contribution experiences a transition and an opposite discontinuity at the SB^d [see (61)]. In (c), the total field (GO + SD + DD) is continuous across the SB^d, at any time, and gradually changes its TD waveform passing from the lit to the shadow region.

IX. Conclusion

A closed form solution for DD fields at a pair of coplanar skew edges has been obtained in Sections II–V. The formulation starts by using analytic signals to handle complex time and

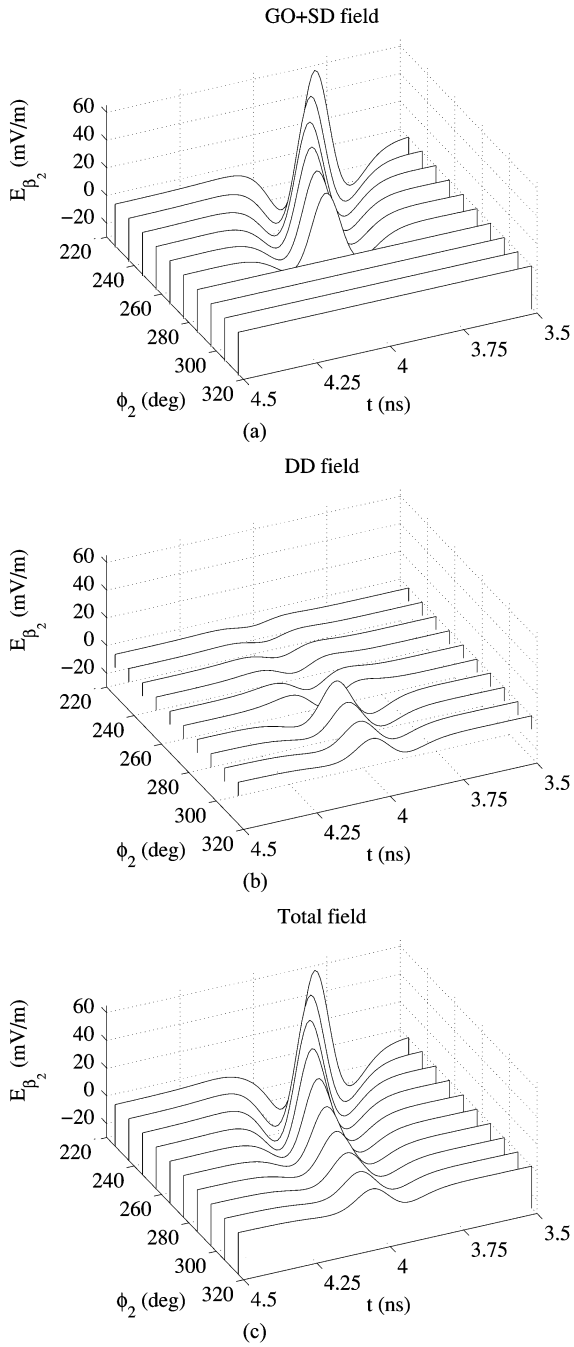

Fig. 11. $\mathbf{u}_{\beta_2}$ component of the transient electric field is plotted along the observation scan in Fig. 9 varying the observation angle ϕ_2. The source dipole is at $\phi_1' = 281°$ (double transition case) and oriented along $\mathbf{u}_{\beta_1'}$, all the geometry and source parameters are shown in Fig. 9. The phenomenology is similar to that in Fig. 10, with the only difference that now the $\mathrm{SB}^{\mathrm{GO}}$ is close to the SB^{d} implying that in (a) the abruptly vanishing SD field is also in its transition. Accordingly, in (b) the DD field has to compensate for that angular discontinuity by experiencing a double transition [see (67)]. In (c), the total field $(\mathrm{GO}+\mathrm{SD}+\mathrm{DD})$ is continuous across the SB^{d}, at any time.

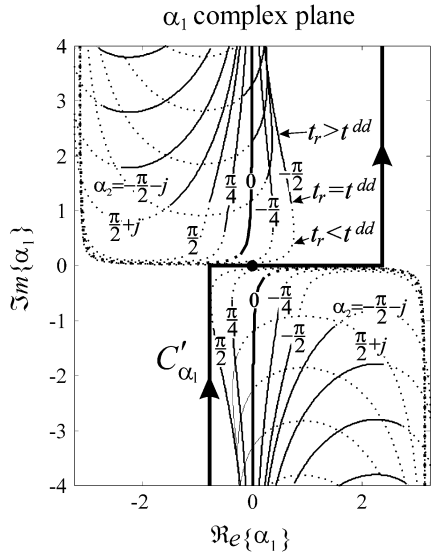

Fig. 12. Complex trajectories of α_1-poles for fixed α_2 values belonging to C'_{α_2} and varying time $t = t_r + jt_i$; with $t_i = 10^{-2}t^{\mathrm{dd}}$. Noncausal $t_r < t^{\mathrm{dd}}$ (dotted line) and causal $t_r > t^{\mathrm{dd}}$ (continuous line) portions of the trajectories are shown. In this example $r_1' = r_2 = 3m$, $\ell = 2m$, $\phi_{12} = \pi/4$, and $\phi_{12}' = \pi/2$. The trajectories never cross the integration path C'_{α_1}.

permit path deformation to prepare the radiation integral for "uniform" and "nonuniform" wavefront approximations. Novel transition functions for TD-DD fields have been determined permitting the uniform description of DD fields near and at the SB of SD rays. It is worth noting that our solution satisfies reciprocity. TD-DD field expressions for the electromagnetic case are obtained by using the scalar solutions to build a dyadic diffraction coefficient defined in the ray fixed coordinate systems. The present TD-DD field is limited to real time and analytic extension of the DD mechanisms to complex time, as in [8], [9], [11] for the SD field, is currently under study. This first investigation lies the foundations to treat subsequent problems involving more general double wedge geometries. The reduction of these TD results for the DD field to the particular case of a flat plate is considered in Section VII.

Numerical results have shown the transitional behavior of TD-DD fields, for various source and observation configurations. It has been also shown, analytically and numerically, how the TD-DD field restores the continuity of the total field $(\mathrm{GO}+\mathrm{SD}+\mathrm{DD}$ fields) across the SB of a SD field. Space limitations have limited our phenomenology discussion to a few representative cases. Closed form results for TD-DD fields excited by particular band limited waveforms can also be obtained and this is left to future investigations. Here we have restricted the analysis to the numerical convolution of the impulse-excited TD-DD with an arbitrary excitation waveform with no low frequency components.

APPENDIX A
COMPLEX TRAJECTORIES OF TD POLES

In this Appendix, using an example, we clarify how the change of variables from the α_1, α_2 to the u, v complex planes and the subsequent integration path deformations are performed. Due to the perfect symmetry between α_1 and α_2, and between u and v, all the following considerations conducted in the α_1 and u complex planes apply also to α_2 and v but are thus not rephrased.

The analytic delta function in (15) introduces time dependent (α_1, α_2)-poles that satisfy (16). The DD field is dominated by the spectral contributions near and at the 2-D stationary point $(\alpha_1, \alpha_2) = (0, 0)$, therefore the following calculations

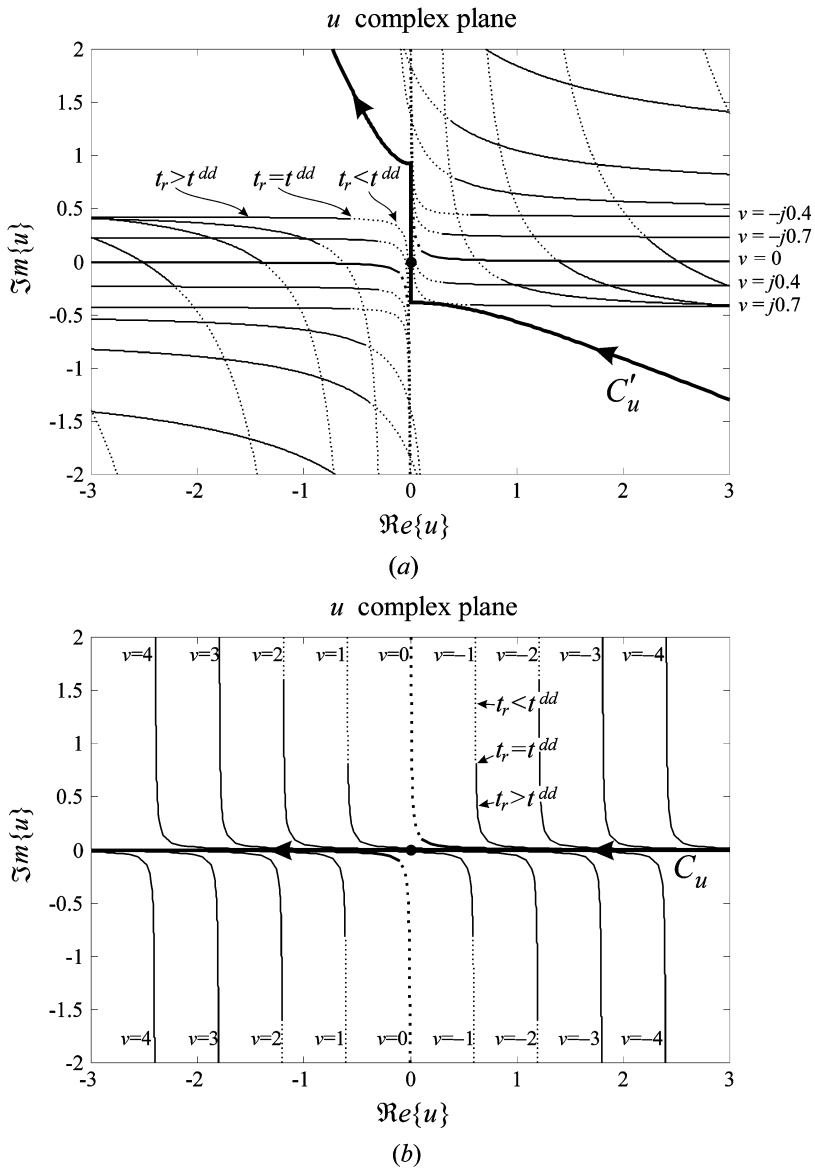

Fig. 13. Complex trajectories of u-poles for fixed v values and varying time $t = t_r + jt_i$; with $t_i = 10^{-2}t^{\rm dd}$. Noncausal $t_r < t^{\rm dd}$ (dotted line) and causal $t_r > t^{\rm dd}$ (continuous line) portions of the trajectories are shown. Values of v belong to (a) integration path C'_v, and (b) the real v-axis. In this example $r'_1 = r_2 = 3m$, $\ell = 2m$, $\phi_{12} = \pi/4$ and $\phi'_{12} = \pi/2$. The, trajectories never cross the integration path (thick gray line) before and after the deformation.

are performed using the quadratic approximation $R(\alpha_1, \alpha_2) \simeq ct^{\rm dd} - (1/2)c\tau_{uu}\sin^2(\alpha_1/2) - c\tau_{uv}\sin(\alpha_1/2)\sin(\alpha_2/2) - (1/2)c\tau_{vv}\sin^2(\alpha_2/2)$ that permits a closed form evaluation of the two α_1-poles symmetric to the origin, as a function of t and α_2. In Fig. 12 the trajectories of the two time-varying poles in the α_1 plane are plotted for various α_2 belonging to the C'_{α_2} contour [see Fig. 3(b)]. To better separate the trajectories, the time $t = t_r + jt_i$ has a small imaginary part $t_i = 10^{-2}t^{\rm dd}$. The dotted and continuous curves show the noncausal $(t_r < t^{\rm dd})$ and causal $(t_r > t^{\rm dd})$ portions of the trajectories, respectively. Note that the trajectories of the α_1-poles never cross the integration path C'_{α_1} (thick gray line). Note also that for $\alpha_2 = 0$, the two trajectories of the two α_1-poles tend to meet at $\alpha_1 = 0$ for $t_r = t^{\rm dd}$ (indeed, this happens exactly only for real time, i.e., when $t_i = 0$) showing that at the wavefront $t = t^{\rm dd}$, the two time dependent pole singularities coincide with the 2-D stationary point $(\alpha_1, \alpha_2) = (0, 0)$ thus providing the main contribution to the DD field.

Once the mapping specified after (19) of the α_1, α_2 planes onto the u, v planes is performed, the time dependent poles are solution of (23), and the trajectories in the u complex plane are shown in Fig. 13(a) for varying $t = t_r + jt_i$, with $t_i = 10^{-2}t_{\rm dd}$. There, for each time t_r, for fixed v, there are two complex poles symmetric to the origin. The thick gray curve represents the contour C'_u, image of C'_{α_1} through the introduced mapping. Again, the dotted and continuous curves show the noncausal $(t_r < t^{\rm dd})$ and causal $(t_r > t^{\rm dd})$ portions of the trajectories, respectively. Since the topology is preserved by the introduced mapping, the trajectories of the u-poles never cross the integration path C'_u, for every value of the v variable that belongs to the C'_v integration path.

After the deformation of both integration paths C'_u and C'_v onto the real u and v axes, respectively, the trajectories of the time dependent u-poles, for fixed v belonging to the real axis, are shown in Fig. 13(b). Again, for each time t_r and fixed v, there are two complex u-poles symmetric to the origin, and the

trajectories of the u-poles never cross the integration path (the u-real axis), for every value of the v variable that belongs to the v-real axis.

In summary, the complex trajectories of the u-poles always lie on the *same* side of the integration path, before and after the deformation of the u- and v-integration paths in the u- and v-planes, respectively. Hence, when *both* integration paths are deformed, time dependent poles are never captured by these deformations.

APPENDIX B

The integrals

$$\mathcal{I}^I = \int_{-\infty}^{\infty}\int_{-\infty}^{\infty} \delta\left[t - \frac{1}{2}(\tau_{uu}u^2 + 2\tau_{uv}uv + \tau_{vv}v^2)\right] du\, dv \tag{74}$$

$$\mathcal{I}^{II} = \int_{-\infty}^{\infty}\int_{-\infty}^{\infty} uv\,\delta\left[t - \frac{1}{2}(\tau_{uu}u^2 + 2\tau_{uv}uv + \tau_{vv}v^2)\right] du\, dv \tag{75}$$

are evaluated as follows. First we introduce in the left-hand side of (74) and (75) the change of variables $u\sqrt{\tau_{uu}/2} = \sigma/\sqrt{1+\nu^2}$ and $v\sqrt{\tau_{vv}/2} = \sigma\nu/\sqrt{1+\nu^2}$, with $du\,dv = (2/\sqrt{\tau_{uu}\tau_{vv}})\cdot\sigma/(1+\nu^2)\,d\sigma\,d\nu$, which respectively leads to

$$\mathcal{I}^I = \frac{2}{\sqrt{\tau_{uu}\tau_{vv}}}\int_{-\infty}^{\infty}\int_{-\infty}^{\infty}\delta\left[t-\sigma^2\frac{p(\nu)}{1+\nu^2}\right]\times\frac{\sigma}{1+\nu^2}\,d\sigma\,d\nu \tag{76}$$

$$\mathcal{I}^{II} = \frac{4}{\tau_{uu}\tau_{vv}}\int_{-\infty}^{\infty}\int_{-\infty}^{\infty}\delta\left[t-\sigma^2\frac{p(\nu)}{1+\nu^2}\right]\times\frac{\sigma^3\nu}{(1+\nu^2)^2}\,d\sigma\,d\nu \tag{77}$$

with $p(\nu) = \nu^2 + 2w\nu + 1$, and w is defined in (42). The inner σ integrals are closed invoking the δ Dirac property $\int f(\sigma)\delta[g(\sigma)]\,d\sigma = \sum_n (f(\sigma_n))/(|g'(\sigma_n)|)$ with σ_n denoting the n-th root of $g(\sigma)$ which lies on the integration path and g' the derivative of g with respect to σ. For $t < 0$, there are no *real* roots and the integrals vanish in accordance with causality. For $t > 0$, there are two *real* roots $\sigma = \pm\sqrt{t(1+\nu^2)/p(\nu)}$ that yield

$$\mathcal{I}^I = \frac{2U(t)}{\sqrt{\tau_{uu}\,\tau_{vv}}}\int_{-\infty}^{\infty}\frac{1}{p(\nu)}\,d\nu \tag{78}$$

$$\mathcal{I}^{II} = \frac{4tU(t)}{\tau_{uu}\tau_{vv}}\int_{-\infty}^{\infty}\frac{\nu}{p^2(\nu)}\,d\nu. \tag{79}$$

The polynomial $p(\nu)$ has conjugate complex roots on the unit circle in Fig. 14. Closing the integration path at infinity in the upper half plane, the integrals (78) and (79) are evaluated as residue contributions at the enclosed pole $\nu_p = -w + j\sqrt{1-w^2}$ (see Fig. 14)

$$\mathcal{I}^I = \frac{2\pi U(t)}{(\tau_{uu}\tau_{vv} - \tau_{uv}^2)^{1/2}}, \quad \mathcal{I}^{II} = \frac{-2\pi tU(t)\tau_{uv}}{(\tau_{uu}\tau_{vv} - \tau_{uv}^2)^{3/2}}. \tag{80}$$

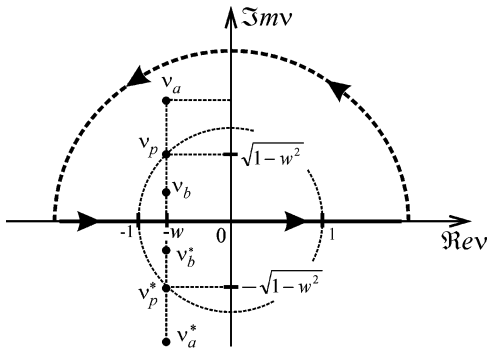

Fig. 14. Topology of the ν complex plane. The integration path on the real axis is closed at infinity in the upper half plane. Integrals (78) and (79) are evaluated as the residue of the pole ν_p. Integrals (83) and (84) are evaluated summing the residues at poles ν_a and ν_b.

APPENDIX C
CLOSED FORM EXPRESSIONS FOR TD-DD TRANSITION FUNCTIONS (38) AND (39)

The evaluation of (38) and (39) is carried out by mapping the ξ,η plane onto the σ,ν plane via the change of variables $\xi = \sigma/\sqrt{1+\nu^2}$ and $\eta = \sigma\nu/\sqrt{1+\nu^2}$, leading to

$$\hat{T}^I\left(\frac{a}{\sqrt{t}},\frac{b}{\sqrt{t}},w\right) = \frac{a^2b^2}{\pi(1-w^2)^{\frac{3}{2}}}\cdot\int_{-\infty}^{\infty}\int_{-\infty}^{\infty}\frac{\delta\left[t-\sigma^2\frac{p(\nu)}{1+\nu^2}\right]}{\left(\frac{\sigma^2}{1+\nu^2}+\frac{a^2}{1-w^2}\right)\left(\frac{\sigma^2\nu^2}{1+\nu^2}+\frac{b^2}{1-w^2}\right)}\times\frac{\sigma}{1+\nu^2}\,d\sigma\,d\nu \tag{81}$$

and

$$\hat{T}^{II}\left(\frac{a}{\sqrt{t}},\frac{b}{\sqrt{t}},w\right) = \frac{-2a^2b^2}{\pi tw\sqrt{1-w^2}}\cdot\int_{-\infty}^{\infty}\int_{-\infty}^{\infty}\frac{\delta\left[t-\sigma^2\frac{p(\nu)}{1+\nu^2}\right]}{\left(\frac{\sigma^2}{1+\nu^2}+\frac{a^2}{1-w^2}\right)\left(\frac{\sigma^2\nu^2}{1+\nu^2}+\frac{b^2}{1-w^2}\right)}\times\frac{\sigma^3\nu}{(1+\nu^2)^2}\,d\sigma\,d\nu \tag{82}$$

with $p(\nu) = \nu^2 + 2w\nu + 1$. The inner-$\sigma$ integrals in (81) and (82) are evaluated as in Appendix A via the time dependent σ roots of the delta function argument. For $t < 0$, there are no *real* roots and the integrals vanish in accordance with causality. For $t > 0$, there are two *real* roots $\sigma = \pm\sqrt{t(1+\nu^2)/p(\nu)}$ which yield

$$\hat{T}^I(\hat{a},\hat{b},w) = U(t)\frac{\sqrt{1-w^2}}{\pi}\int_{-\infty}^{\infty}\frac{p(\nu)}{Q(\nu)}\,d\nu \tag{83}$$

and

$$\hat{T}^{II}(\hat{a},\hat{b},w) = U(t)\frac{-2(1-w^2)^{\frac{3}{2}}}{\pi w}\int_{-\infty}^{\infty}\frac{\nu}{Q(\nu)}\,d\nu \tag{84}$$

where we have introduced the *nondimensional* parameters $\hat{a}(t) = a/\sqrt{t}$, $\hat{b}(t) = b/\sqrt{t}$ (recall that $t > 0$) which completely account for the t-dependence, and $Q(\nu) = [p(\nu) + (1-w^2)/\hat{a}^2][p(\nu) + \nu^2(1-w^2)/\hat{b}^2]$ is

a polynomial. Due to the vanishing behavior of the integrand when $|\nu| \to \infty$, the integration path in both (83) and (84) is closed at infinity in the upper half plane. The integrals (83), (84) are evaluated as the sum of the residue contributions at the two enclosed poles $\nu_a = -w + j\sqrt{1-w^2}\sqrt{1+\hat{a}^{-2}}$ and $\nu_b = (-w - j\sqrt{1-w^2}\sqrt{1+\hat{b}^{-2}})^{-1}$ (see Fig. 14), leading to the closed form TD transition functions (43) and (44). Note that at the DD wavefront, the time-dependent poles ν_a and ν_b coalesce at ν_p, whereas for $t > t^{\mathrm{dd}}$ they move apart as depicted in Fig. 14, and when $t \to \infty$, $\nu_a \to -w + j\infty$ and $\nu_b \to 0$

ACKNOWLEDGMENT

The authors would like to thank Prof. R. Tiberio and Prof. L. B. Felsen for introducing them to the marvelous double diffraction and transient worlds, respectively, and they are thankful to Prof. E. Heyman for his useful comments and suggestions on the spectral TD formulation.

REFERENCES

[1] J. B. Keller and A. Blank, "Diffraction and reflection of pulses by wedges and corners," *Comm. Pure Appl. Math.*, vol. 4, pp. 75–94, 1951.
[2] L. B. Felsen, "Diffraction of the pulsed field from an arbitrarily oriented electric or magnetic dipole by a perfectly conducting wedge," in *SIAM J. Appl. Math.*, vol. 26, Mar. 1974, pp. 306–312.
[3] L. B. Felsen and N. Marcuvitz, *Radiation and Scattering of Waves*. Englewood Cliffs, NJ: Prentice-Hall, 1973.
[4] E. Heyman and L. B. Felsen, "Weakly dispersive spectral theory of transients: Part I—Formulation and interpretation," *IEEE Trans. Antennas Propag.*, vol. 35, no. 1, pp. 80–86, Jan. 1987.
[5] ——, "Weakly dispersive spectral theory of transients, part II: Evaluation of the spectral integral," *IEEE Trans. Antennas Propag.*, vol. 35, no. 5, pp. 574–580, May 1987.
[6] E. Heyman, "Weakly dispersive spectral theory of transients: Part III—Applications," *IEEE Trans. Antennas Propag.*, vol. 35, no. 11, pp. 1258–1266, Nov. 1987.
[7] T. W. Veruttipong, "Time domain version of the uniform GTD," *IEEE Trans. Antennas Propag.*, vol. 38, no. 11, pp. 1757–1764, Nov. 1990.
[8] R. Ianconescu and E. Heyman, "Pulsed field diffraction by a perfectly conducting wedge: A spectral theory of transients analysis," *IEEE Trans. Antennas Propag.*, vol. 42, no. 6, pp. 781–789, Jun. 1994.
[9] ——, "Pulsed beam diffraction by a perfectly conducting wedge: Exact solution," *IEEE Trans. Antennas Propag.*, vol. 42, no. 10, pp. 1377–1385, Oct. 1994.
[10] E. Heyman and R. Inconescu, "Pulsed beam diffraction by a perfectly conducting wedge: Local scattering models," *IEEE Trans. Antennas Propag.*, vol. 43, no. 5, pp. 519–528, May 1995.
[11] P. R. Rousseau and P. H. Pathak, "Time-domain uniform geometrical theory of diffraction for a curved wedge," *IEEE Trans. Antennas Propag.*, vol. 43, no. 12, pp. 1375–1382, Dec. 1995.
[12] F. Capolino, M. Albani, S. Maci, and R. Tiberio, "Double diffraction at a pair of coplanar skew edges," *IEEE Trans. Antennas Propag.*, vol. 45, no. 8, pp. 1219–1226, Aug. 1997.
[13] M. Albani, P. Piazzesi, F. Capolino, S. Maci, and R. Tiberio, "Shielding effect of a thick screen with corrugations," *IEEE Trans. Electrom. Compat.*, vol. 40, no. 3, pp. 235–239, Aug. 1998.
[14] M. Albani, F. Capolino, S. Maci, and R. Tiberio, "Double diffraction at a pair of coplanar skew wedges," presented at the IEEE APS Symp., Orlando, FL, Jul. 11–16, 1999.
[15] ——, "Diffraction at a thick screen including corrugations on the top face," *IEEE Trans. Antennas Propag.*, vol. 45, no. 2, pp. 277–283, Feb. 1997.
[16] F. Capolino and M. Albani, "Impulsive pyramid-vertex and double-wedge diffraction coefficients," presented at the IEEE AP-S Symp., Boston, MA, Jul. 8–13, 2001.
[17] P. C. Clemmow and T. B. A. Senior, "A note on a generalized Fresnel integral," in *Proc. Cambridge Phil. Soc.*, vol. 49, 1953, pp. 570–572.
[18] H. Shirai and L. B. Felsen, "Wavefront and resonance analysis of scattering by a perfectly flat strip ," *IEEE Trans. Antennas Propag.*, vol. AP-34, no. 10, pp. 1196–1207, Oct. 1986.
[19] ——, "Spectral method for multiple edge diffraction by a flat strip," *Wave Motion*, vol. 8, pp. 449–524, 1986.
[20] F. Capolino and S. Maci, "Uniform high-frequency description of singly, doubly, and vertex diffracted rays for a plane angular sector," *J. Electromagn. Wave Applicat.*, vol. 10, no. 9, pp. 1175–1197, Oct. 1996.
[21] ——, "Simplified, closed-form expressions for computing the generalized Fresnel integral and their application to vertex diffraction," *Microw. Opt. Technol. Lett.*, vol. 9, no. 1, pp. 32–37, May 1995.
[22] R. Tiberio, G. Manara, G. Pelosi, and R. Kouyoumjian, "High-frequency electromagnetic scattering of plane waves form double wedges," *IEEE Trans. Antennas Propag.*, vol. 37, no. 9, pp. 1172–1180, Sep. 1989.
[23] M. Schneider and R. Luebbers, "A general UTD diffraction coefficient for two edges," *IEEE Trans. Antennas Propag.*, vol. 39, no. 1, pp. 8–14, Jan. 1991.
[24] L. P. Ivrissimitzis and R. J. Marhefka, "Double diffraction at a coplanar skewed egde configuration," *Radio Sci.*, vol. 26, pp. 821–830, 1991.
[25] R. G. Kouyoumjian and P. H. Pathak, "A uniform geometrical theory of diffraction for an edge in a perfectly conducting surface," *Proc. IEEE*, vol. 62, no. 11, pp. 1448–1461, Nov. 1974.
[26] S. W. Lee and J. Boersma, "Ray-optical analysis of fields on shadow boundaries of two paralle plates," *J. Math. Phys.*, vol. 16, no. 5, pp. 1746–1764, 1975.
[27] R. Tiberio and R. Kouyoumjian, "A uniform GTD solution for the diffraction by strips illuminated at grazing incidence," *Radio Sci.*, vol. 14, pp. 933–941, 1979.
[28] ——, "High-frequency electromagnetic scattering of plane waves form double wedges," *Radio Sci.*, vol. 17, pp. 323–336, 1982.

Filippo Capolino (S'94–M'97–SM'04) was born in Florence, Italy, in 1967. He received the Laurea degree (*cum laude*) in electronic engineering and the Ph.D. degree from the University of Florence, Italy, in 1993 and 1997, respectively.

From 1994 to 2000, he was a Lecturer of antennas at the Diploma di Laurea, University of Siena, Italy, where he has been a Research Associate until 2002 and presently employed as an Assistant Professor. From 1997 to 1998, he was a Fulbright Research Visitor with the Department of Aerospace and Mechanical Engineering, Boston University, Boston, MA, where he continued his research with a Grant from the Italian National Council for Research (CNR), from 1998 to 1999. From 2000 to 2001, he was Research Assistant Visiting Professor with the Department of Electrical and Computer Engineering, University of Houston, Houston, TX, where he is now an Adjunct Assistant Professor. In November to December 2003, he was an Invited Assistant Professor at the Institut Fresnel, Marseille, France. His primary research interests is in high-frequency, short-pulse radiation, array antennas, periodic structures, and metamaterials. He is the coordinator of the Siena Unit for the Network of Excellence "Metamorphose" on Metamaterials of the EU FP6.

Dr. Capolino was awarded with a MMET'94 Student Paper Competition Award in 1994, the Raj Mittra Travel Grant for Young Scientists in 1996, the "Barzilai" prize for the best paper at the National Italian Congress of Electromagnetism (XI RiNEm) in 1996, and a Young Scientist Award for participating at the URSI International Symposium on Electromagnetics. Theory in 1998. He received the R. W. P. King Prize Paper Award from the IEEE Antennas and Propagation Society for the Best Paper of the Year 2000, by an author under 36. He is an Associate Editor for the IEEE TRANSACTIONS OF ANTENNAS AND PROPAGATION.

Matteo Albani (M'98) was born in Florence, Italy, on January 5, 1970. He received the Laurea degree in electronic engineering and the Ph.D. degree in telecommunications and electronic engineering from the University of Florence, Italy, in 1994 and 1998, respectively.

From 1999 to 2001, he was an Associate Researcher with the Dept. of Information Engineering, University of Siena, Italy. Since 2001 he has been associated with the Dept. of Matter Physics and Advanced Physical Technologies, University of Messina, Italy, where he is currently an Assistant Professor. His research interests encompass high-frequency methods for electromagnetic scattering and propagation, numerical methods for large array antennas, antenna analysis and design.

Dr. Albani was awarded with the "Giorgio Barzilai" prize for the best young scientist paper at the Italian National Conference on Electromagnetics in 2002 (XIV RiNEm).